TECHNICAL REPORT
NATICK/TR-03/006

AD_____

DEVELOPMENT OF A DYNAMIC NUTRITION MODEL (DYNUMO)

by
Tammy J. Doherty

Simulation Technologies, Inc.
Dayton, OH 45402-1106

November 2002

Final Report
February 2000 – December 2000

Prepared for
U.S. Army Soldier and Biological Chemical Command
Soldier Systems Center
Natick, Massachusetts 01760-5020

DISCLAIMERS

The findings contained in this report are not to be construed as an official Department of the Army position unless so designated by other authorized documents.

Citation of trade names in this report does not constitute an official endorsement or approval of the use of such items.

DESTRUCTION NOTICE

For Classified Documents:

Follow the procedures in DoD 5200.22-M, Industrial Security Manual, Section II-19 or DoD 5200.1-R, Information Security Program Regulation, Chapter IX.

For Unclassified/Limited Distribution Documents:

Destroy by any method that prevents disclosure of contents or reconstruction of the document.

REPORT DOCUMENTATION PAGE

Form Approved
OMB No. 0704-0188

1. REPORT DATE *(DD-MM-YYYY)*	2. REPORT TYPE	3. DATES COVERED *(From - To)*
14-11-02	FINAL	February 2000- December 2000

4. TITLE AND SUBTITLE
DEVELOPMENT OF A DYNAMIC NUTRITION MODEL (DYNUMO)

5a. CONTRACT NUMBER
DAAD16-99-C-1003

5b. GRANT NUMBER

5c. PROGRAM ELEMENT NUMBER

6. AUTHOR(S)
Tammy J. Doherty

5d. PROJECT NUMBER
25151V

5e. TASK NUMBER

5f. WORK UNIT NUMBER

7. PERFORMING ORGANIZATION NAME(S) AND ADDRESS(ES)
Simulation Technologies, Inc.
111 West First Street
Suite 748
Dayton, OH 45402-1106

8. PERFORMING ORGANIZATION REPORT NUMBER

9. SPONSORING/MONITORING AGENCY NAME(S) AND ADDRESS(ES)
U.S. Army Soldier and Biological Chemical Command
Soldier Systems Center
Natick, MA 01760-5020

10. SPONSOR/MONITOR'S ACRONYM(S)
SBCCOM

11. SPONSOR/MONITOR'S REPORT NUMBER(S)
NATICK/TR-03/006

12. DISTRIBUTION/AVAILABILITY STATEMENT
Approved for public release; distribution is unlimited

13. SUPPLEMENTARY NOTES

14. ABSTRACT

Performance of the warrior system depends to a great extent on the physical and cognitive capabilities of the warfighter. Metabolic fuel status is one factor that can be directly linked to those performance capabilities. This report describes the development of a dynamic nutrition model (DYNUMO) that simulates body metabolic fuel levels over time, in response to nutrient intake and energy expenditure. DYNUMO is a simplification of the digestive and metabolic processes in the human body. Ingested food is absorbed into the blood. From there, absorbed nutrients may be stored in adipose tissue as triglycerides, stored in the liver or muscle as glycogen, converted to other metabolic fuels in the liver or utilized for energy. A regulatory system maintains blood glucose at near constant levels and conserves carbohydrate stores. Model algorithms are based on known physiology and biochemistry, with parameter values derived from existing experimental data. Although insufficient data were available for formal model validation, the model currently provides reasonable predictions of blood glucose levels following a single ingestion of a carbohydrate solution and of muscle glycogen levels following a single exercise bout. The model has not been fully tested, however, and it is likely that parameter values and the level of model detail will require adjustment in the future.

15. SUBJECT TERMS

NUTRITION	PREDICTIONS	MILITARY NUTRITION	CARBOHYDRATES
MODELING	DIGESTION (BIOLOGY)	SIMULATION	DEPLETION
METABOLISM	RATION INTAKE	BIOCHEMISTRY	

16. SECURITY CLASSIFICATION OF:			17. LIMITATION OF ABSTRACT	18. NUMBER OF PAGES	19a. NAME OF RESPONSIBLE PERSON
a. REPORT	b. ABSTRACT	c. THIS PAGE			Paul Short
U	U	U	SAR	93	19b. TELEPHONE NUMBER *(Include area code)* 508-233-4256

TABLE OF CONTENTS

CONTENTS CONT'D

CONTENTS CONT'D

LIST OF FIGURES

LIST OF TABLES

TABLES CONT'D

PREFACE

Development of the Dynamic Nutrition Model (DYNUMO), described in this report, is part of a larger modeling effort to assess the effects of nutrition, ration intake scheduling, and fatigue on military operations. This report covers the period February 2000 to December 2000 and details the work on the DYNUMO model performed under Natick Contract DAAD16-99-C-1003 by Simulation Technologies Inc. (STI) of Dayton, OH 45402-1106. Work on the DYNUMO model began with a literature review to obtain the necessary background information. Meetings were arranged with Irwin Taub, Senior Scientist, US Army Soldier Center, Natick, MA and with Reed Hoyt, Research Scientist and Science Technology Objective (STO) Manager, Warfighter Physiological Status Monitor, U.S. Army Research Institute of Environmental Medicine, Natick, MA, to obtain a better understanding of the problems of military nutrition, and nutritional physiology, and biochemistry. From these discussions and from the literature review, it became clear that carbohydrate depletion is the primary limiting factor for military tasks requiring physical exertion and affects cognitive and emotional well-being during prolonged, exhausting military training exercises. Balancing protein anabolism and catabolism typically increases in importance after several days as well. The importance of tracking total carbohydrate stores, muscle carbohydrate stores, and the relative amounts of carbohydrate and fat metabolism was emphasized. From this background material and these discussions, it was determined that a mathematical model based on known physiology and biochemistry was required. This model needed to be of sufficient resolution to examine interactions among carbohydrate, fat, and protein metabolism. Furthermore, the model needed to be dynamic to estimate the effects of nutritional intake and energy expenditure over time.

In addition to the literature review to obtain background information, a literature search was conducted to identify any existing models meeting project requirements. After a review of the published models, it was determined that none could provide the required scope and resolution.

Model development commenced in March 2000 using Matlab/Simulink development software (The Mathworks, Natick, MA). The model was initially based on the textbook "Biochemistry for the Medical Sciences" by Newsholme and Leech (1983), which is complete in providing both kinetic equations and information regarding metabolic regulation. The textbook "Biochemistry" by Stryer (1995) provided updated information, particularly to the kinetic equations. Initial model coding, for all submodels, was completed in May 2000. Initial parameter value identification and submodel testing for the Central Blood Compartment, Regulatory System, Digestive System and Metabolically-Active Tissue submodels was completed in December 2000.

The model was briefed in detail to Paul Short, STO Manager for Warrior Systems Modeling Technology at Natick, and Mr. Taub in April 2000. The model was also briefed to the Food and Nutrition Research and Engineering Board (FNREB) in June 2000. A two-page project summary was submitted to the Army Science Conference (ASC) and was accepted for poster presentation. The poster was presented at the ASC in

December 2000. The corresponding full paper is published in the Proceedings of the Army Science Conference in 2001.

This report describes all work conducted through December 31, 2000. As of that date, parameter value identification and submodel testing had been conducted only for scenarios that included glucose ingestion and single exercise bouts. It is recommended that the version of the model described in this report be used only for these types of scenarios.

ACKNOWLEDGEMENTS

The project described in this report would not have been possible without the efforts of numerous groups and individuals. Vic Middleton of Simulation Technologies Inc. has provided guidance throughout this research and has been instrumental in defining the usability requirements. Messrs. Dale Malabarba, Paul Short, Medhat Korna and the Modeling and Analysis Team, Natick Soldier Center, have kept the project moving forward and provided whatever support was required. Mr. Hoyt of the U.S. Research Institute of Environmental Medicine and Mr. Taub of the Natick Soldier Center provided background information on the relevant physiology. Gerald Darsch, Director of Combat Feeding Directorate and the Food and Nutrition group, Natick Soldier Center, have provided general support and valuable feedback. Special recognition goes to Patrick Dunne (Natick) and to Elizabeth Meurer (STI) for providing the technical review.

DEVELOPMENT OF A DYNAMIC NUTRITION MODEL

EXECUTIVE SUMMARY

Performance of the warrior system depends to a great extent, on the physical and cognitive capabilities of the warfighter. Physical and cognitive performance capabilities are linked directly to metabolic fuel status, among other factors. This report describes The Development Of A Dynamic Nutrition Model (DYNUMO) that simulates body metabolic fuel status over time, in response to nutrient intake and energy expenditure. This model is part of a larger modeling effort to assess the effects of nutrition, ration scheduling, and fatigue on military operations.

DYNUMO is a simplification of the digestive and metabolic processes in the human body. Model algorithms are based on known physiology and biochemistry, with parameter values derived from existing experimental data. The level of resolution is intended to be just sufficient to predict changes in metabolic fuel status, over time, in response to nutrient intake and physical activity. Submodels include the Central Blood Compartment, Digestive System, Metabolically-Active Tissue, Adipose Tissue, Liver Tissue, and Regulatory System.

The Central Blood Compartment is the common interface for all other submodels within DYNUMO. Nutrients are absorbed into the blood from the Digestive System. From there nutrients may be stored in Adipose Tissue as triacylglycerols, stored in the Liver Tissue or muscle (Metabolically-Active Tissue) as glycogen, converted to other metabolic fuels in Liver Tissue, or used for energy within Metabolically-Active Tissue. The Regulatory System changes the levels of central regulatory factors (e.g., epinephrine, insulin, and glucagon) that adjust nutrient availability to meet metabolic demands and regulate the blood glucose level.

The Digestive System submodel includes the ingestion and gastric emptying of carbohydrates, fats and proteins, plus digestion and absorption of carbohydrates and fats. Protein digestion and absorption are not considered at this time. The ingestion process assumes that food is consumed as a bolus. A modification of the model described by Hunt and Stubbs (1975) is used to describe gastric emptying. A simple pipeline model with constant coefficients is used to describe digestion and absorption.

Metabolically-Active Tissue includes all the cells in the body that consume metabolic fuels to perform physiological work (e.g., muscle contraction, active membrane transport and biosynthesis). Because muscle makes up the greatest percentage of Metabolically-Active Tissue by weight and is responsible for nearly all of the energy consumption that occurs during physical activity, muscle cell characteristics are used to represent Metabolically-Active Tissue. Glucose metabolism, fatty acid metabolism, and the pathways common to both are included in the model. Amino acid and ketone body

metabolism are not currently included. Most of the biochemical pathway models are based on the quasi-steady-state model of Briggs and Haldane (1925). In some cases, a very fast reaction rate is assumed, in which case a maximal, substrate-limited model is used.

The Adipose Tissue submodel includes processes for the uptake of fatty acids and glucose from the blood, and the conversion of these nutrients into triacylglycerol for storage. Conversion of triacylglycerol into glycerol and fatty acids, for release into the blood, is also considered.

The Liver Tissue submodel includes processes for converting and storing metabolic fuels for use by other tissues Liver Tissue takes up glucose, amino acids, fatty acids, glycerol, and lactate, and converts these into glucose by the process of gluconeogenesis. The liver stores glycogen in a manner similar to the Metabolically-Active Tissue. However, unlike its use in Metabolically-Active Tissue, this glycogen can be converted back to glucose and released into the blood for use by other tissues. Fatty acid metabolism (e.g., TriG production and storage, ketogenesis, and VLDL production) is currently ignored.

The Regulatory System controls the release of centrally-produced or centrally-acting factors that affect nutrient transport and metabolism. DYNUMO currently incorporates models for insulin, glucagon, and epinephrine production and release.

This report describes work completed between February and December 2000. Progress during this period included the development of the mathematical model and implementation of mathematical equations in the Matlab Simulink environment. Parameter value estimation and model testing were completed for the Central Blood Compartment, Regulatory System, Digestive System and Metabolically-Active Tissue submodels. The model has not been fully tested and it is likely that parameter values and the level of model detail will require adjustment in the future.

INTRODUCTION

Performance of the warrior system depends not only on equipment, clothing, and weapon systems, but also on physical and cognitive capabilities. Physical and cognitive capabilities are directly related to the levels of metabolic fuels stored in the body, among other factors. Carbohydrate is the most important of these fuels for physical and cognitive performance. Depletion of carbohydrate stored as muscle glycogen is associated both with loss of muscle strength (Jacobs et al., 1981) and with the onset of physical exhaustion (Ahlborg et al., 1967; Bergstrom and Hultman, 1967; Hermansen et al., 1997; Jacobs et al., 1997) and reductions in cognitive performance (Benton et al., 1995; Cox et al., 1993; Holmes et al., 1986; Parker and Benton, 1995). When muscle glycogel levels are low, it is still possible to perform low intensity work. Although not as readily available for physical work as muscle glycogen, lever glycogen is another important form of carbohydrate because it can be converted to glucose and released into the blood to help maintain normal blood glucose levels.

Compared to the body's carbohydrate stores, the body's fat stores are abundant. Although fat cannot provide all the fuel required for high intensity work, fat can be used almost exclusively during low intensity work and can be used to supplement carbohydrate fuels during high intensity work. Protein is also relatively plentiful in the body. Under conditions of prolonged or severe caloric deficits, the body can catabolize protein for metabolic fuel. Unlike carbohydrate and fat catabolism however, excessive protein catabolism is deleterious because the protein comes from the breakdown of body tissue. Loss of greater than 50% of the body's protein generally results in death.

The goal of the ration developer is straightforward: design/develop ration components and schedules to meet the body's nutritional demands during military operations. The conditions associated with military operations however, make achieving this goal difficult at best. Military operations are often measured in terms of days or weeks. The operational environment may be at the extremes of heat, cold, or altitude tolerance. Sleep deprivation and other stresses are often factors as well. Daily caloric expenditures typically far exceed daily caloric intake, which may be limited by the amount of food that can be carried, the amount of time allocated for eating, and by the palatability/acceptance of foods necessarily developed with high priority on low weight/volume and long shelf life (Marriott, 1995). Designing and developing ration components and ration schedules to meet nutritional requirements under such conditions is a considerable challenge.

The Dynamic Nutrition Model (DYNUMO), described in this report, assists the efforts of ration developers by predicting the dynamic response of the body's metabolic fuel stores to various nutrient intake and energy expenditure scenarios. DYNUMO is intended to be used with ration optimization algorithms and force-on-force models alongside algorithms that predict physical and cognitive performance capabilities from metabolic fuel status. Using these tools ration developers can assess the effects of various rations or ration schedules on metabolic fuel status and performance for a wide variety of scenarios. The DYNUMO version described in this report is limited in functionality. The Digestive System and Metabolically-Active Tissue submodels are relatively complete. The Liver

Tissue and Adipose Tissue submodels require parameter estimation and submodel testing. The model has been tested for glucose ingestion and single bouts of exercise and it is recommended that the model be used only for these types of scenarios for the present time.

MODEL OVERVIEW

Objectives

The project described in this report is part of a larger modeling effort to assess the effects of nutrition, ration intake scheduling, and fatigue on military operations. The objective of the DYNUMO component is to track the effects of nutrient intake and energy expenditure on body metabolic fuel status over time. DYNUMO will be deployed as an algorithm to be called by another program.

Requirements

Most of the metabolic fuels that are taken up and metabolized by cells are used to convert adenosine diphosphate (ADP) to adenosine triphosphate (ATP). ATP provides energy for muscle contraction, membrane transport, and biosynthetic processes. The ATP concentration in muscle is approximately 4.0 mM (Stryer, 1995, p. 448), which is enough to sustain muscle contraction for less than one second (Stryer, 1995, p. 448). Because of the limited steady-state amount of cellular ATP, except for very brief periods of time, ATP production must keep pace with ATP expenditure. Metabolic fatigue occurs when the ATP production is inadequate to sustain cellular processes.

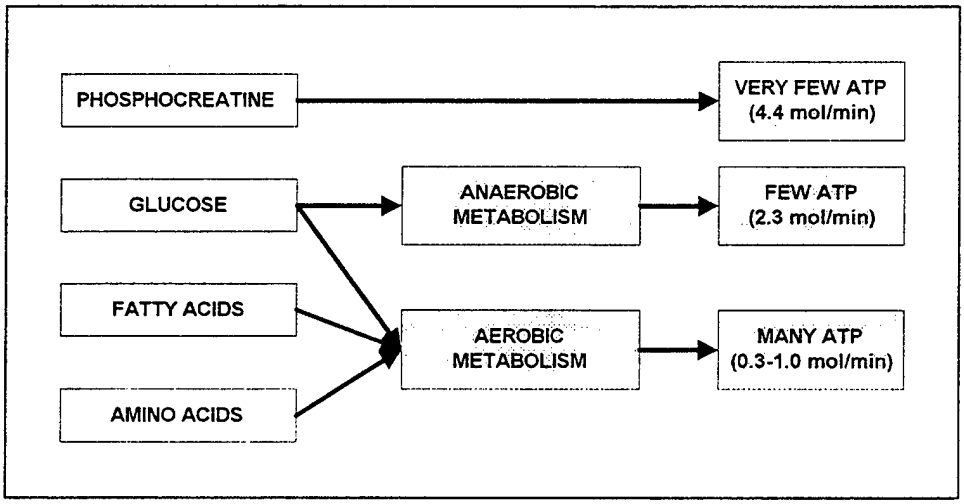

Figure 1 - Rates Of ATP Production For Various Metabolic Fuels

Rates of ATP production depend on the metabolic fuel that is used (Figure 1- adapted from Burke, 1999, Fig 2.2, p.21). In the muscle, phosphocreatine and muscle glycogen can be used to generate ATP via anaerobic metabolism at the fastest rates (4.4 and 2.3 mol/min, respectively (Stryer, 1995, p. 778)) and are the primary fuels for "all-out," maximal efforts. Muscle glycogen, liver glycogen, and adipose tissue fatty acids generate ATP, via aerobic metabolism, at slower rates of 1.0, 0.37, and 0.40 mol/min, respectively (Stryer, 1995, p. 778). Fatty acids produce ATP at the slowest rate and, used alone, can support only low to moderate levels of physical activity. For higher activity levels, a mixture of fuels that includes greater contributions of muscle glycogen must be

used (see Table 1from Newsholme et al., 1992). Because the muscle glycogen supply is limited, the primary limiting factor for prolonged muscle activity is muscle glycogen depletion (Hultman, 1967). During anaerobic metabolism, muscular activity is also limited by the slowing down of the metabolic pathway due to low pH levels resulting from lactate and hydrogen ion accumulation.

Table 1 - Estimation of the contribution of different fuels to ATP generation for various running events

		Glycogen			
Event	***Phosphocreatine***	***Anaerobic***	***Aerobic***	***Blood Glucose***	***Fatty Acids***
100 m	50	50			
200 m	25	65	10		
400 m	12.5	62.5	25		
800 m	6	50	44		
1500 m	[a]	25	75		
5000 m	[a]	12.5	87.5		
10000 m	[a]	3	97		
Marathon			75	5	20
Ultra Marathon (80 km)			35	5	60
24-h race			10	2	88
Soccer Game	10	70	20		

[a] Phosphocreatine used during the first few seconds and, if resynthesized during the race, during the final sprint.

The brain requires approximately 120g of glucose per day and accounts for 60% of the energy metabolism at rest (Stryer, 1995, p. 770). The brain does not store metabolic fuels and can use only glucose and ketone bodies (derived from protein and lipid metabolism) to support cellular activities for energy. Therefore, the brain depends upon an adequate blood glucose supply. Glycolysis in the brain slows when the blood glucose level is below approximately 2.2 mM (Stryer, 1995, p. 770). Liver glycogen is the reservoir used to maintain normal blood glucose levels. In terms of metabolic fuels, the amount of stored liver glycogen is a limiting factor for cognitive performance.

It is clear that depletion of ATP in the cell leads to metabolic fatigue. ATP depletion occurs when ATP expenditure exceeds ATP generation from metabolic fuels. To evaluate different nutritional strategies on physical and cognitive performance, DYNUMO must keep track of the status (i.e., the amounts and rates of utilization and replenishment) for the various metabolic fuels. Although carbohydrate fuels are the primary limiting factors for performance, tracking the availability of non-carbohydrate fuels is also important because they affect the rates of utilization of carbohydrate during mixed metabolism.

Scope

This model will focus on the problem of military operations that last from hours to days. Under these conditions, the following metabolic fuel stores contribute significantly to ATP generation: adipose tissue triacylglycerol, liver glycogen, muscle glycogen, blood glucose, and blood fatty acids. The current emphasis is on carbohydrate metabolism,

because carbohydrate availability is the primary limiting factor for performance. Although protein metabolism and ketone body metabolism occur nearly continuously, these only become important after prolonged states of carbohydrate inadequacy and are not considered at this time. Similarly, muscle phosphocreatine metabolism is important only in the first few seconds of all-out efforts and is also not considered for now. The model is based on known biochemistry, but is at a level of detail that is just sufficient to describe the physiology.

General Model Description

DYNUMO is a simplified description of the metabolic processes in the human body. Inputs to the model include the amount and complexity of ingested food (carbohydrate and fat), the rate of energy expenditure, and a stress (epinephrine) factor over time. Outputs include the overall caloric balance as well as the metabolic fuel status (i.e., muscle and liver glycogen, adipose triacylglycerol, blood glucose, and blood free fatty acids) over time. Ingested food enters the digestive tract and is broken down into its basic components. The volume and macronutrient complexity of the food determine the rate of digestion. These basic nutrient components are then absorbed into the blood. From there, nutrients are stored in adipose tissue as triacylglycerol, stored in the liver or muscle as glycogen, converted to other metabolic fuels in the liver, or utilized for energy. A regulatory system adjusts insulin and glucagon levels to maintain blood glucose at or near constant levels and to conserve carbohydrate stores. Model algorithms are based on known physiology and biochemistry, with parameter values derived from known system behavior and from existing experimental data. A schematic of the model is shown below in Figure 2. Each compartment (i.e., Blood, Digestive System, Adipose Tissue, Liver Tissue, Metabolically-Active Tissue, and Regulatory Center) is treated as a separate submodel and is described in a separate section of this report. The remainder of this section describes the elements that are common to all of the submodels.

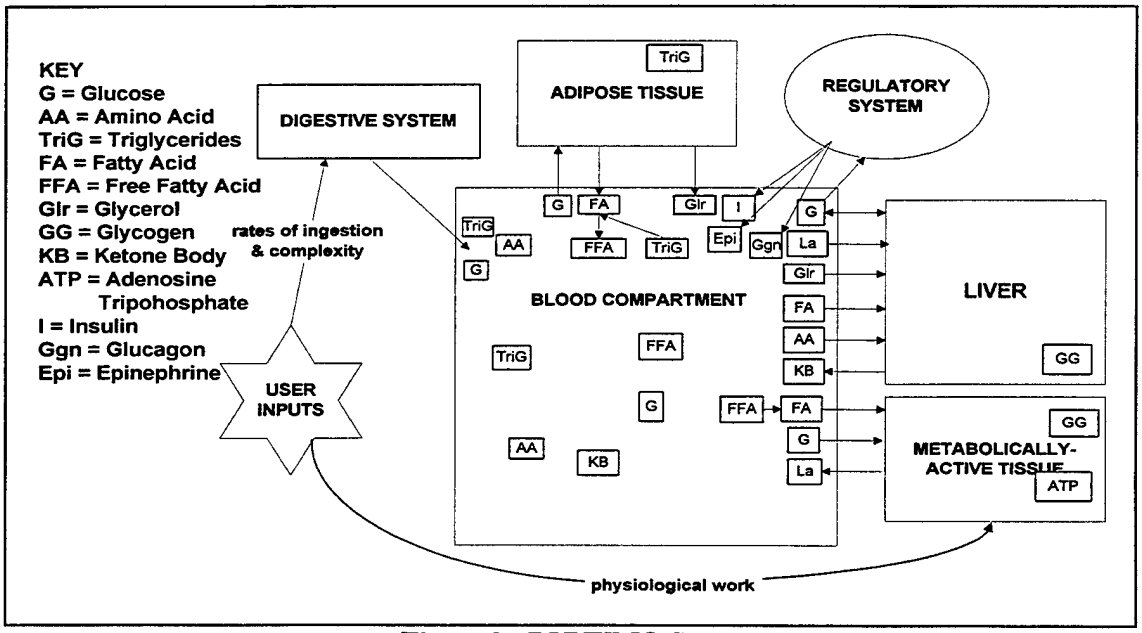

Figure 2 - DYNUMO Schematic

Metabolic Pathway Models

Metabolic biochemistry is highly complex, incorporating numerous individual metabolic pathways that interact with one another. A metabolic pathway typically includes multiple steps, each catalyzed by a specific enzyme. In DYNUMO, all steps in a pathway are collapsed into a single, net reaction. The reaction rate and regulation scheme for the pathway are assigned the properties of the enzyme catalyzing the rate-determining step. For example, the glycolytic pathway that converts glucose 6-phosphate to pyruvate is a multi-step process that is treated as a single reaction in the model. The reaction rate and regulation scheme are assigned the properties of 6-phosphofructokinase, which catalyzes the rate-determining step.

Four types of pathway models are used: models based on the law of mass action, pipeline models, quasi-steady-state saturation kinetic models, and maximal, substrate-limited models.

Models Based on the Law of Mass Action

Models based on the law of mass action assume that the rate of product formation (dP/dt) or the "reaction rate," is directly proportional to the substrate concentration ([S]) by a proportionality coefficient, k:

$$\frac{dP}{dt} = k \cdot [S]$$

In the case of n substrates, the equation above may be expanded to:

$$\frac{dP}{dt} = k \cdot [S_1] \cdot [S_2] ... [S_n]$$

Pipeline Model

A pipeline model is an extension of the mass action model. The pipeline model assumes that the substrate, S_0, is converted to P in two or more steps, each governed by the law of mass action. Substrate flows into the system at rate R.

$$\begin{array}{l} R \\ \downarrow \\ S_0 \xrightarrow{k_0} S_1 \xrightarrow{k_1} S_2 \xrightarrow{k_2} S_3 \xrightarrow{k_3} ... S_n \xrightarrow{k_n} P \end{array}$$

We assume that the volume is the same for each segment in the pipeline so that substrates (S) and product (P) may be expressed as amounts instead of as concentrations. We also assume that the rate coefficients are the same for each segment (i.e., $k_i = k$).

The corresponding rate equations are:

$$\frac{dS_0}{dt} = R - kS_0$$
$$\frac{dS_i}{dt} = +k(S_{i-1} - S_i), \quad 1 \le i \le n$$
$$\frac{dP}{dt} = +kS_n$$

The solution for the first substance (S_0) is a decaying exponential. The solution for S_1 contains two exponentials. The solution for S_3 contains three exponentials, and so on.

Quasi-Steady-State Saturation Kinetic Models

Saturation kinetic models are used when there is a limited supply of either enzyme (E) or substrate (S):

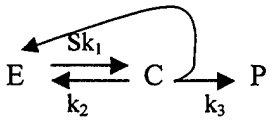

This model assumes that S and E combine to form an enzyme-substrate complex, C. k_i values are rate coefficients for the individual reactions are assumed to be governed by the law of mass action. The resulting set of equations is provided below.

$$\frac{dE}{dt} = -k_1 ES + (k_2 + k_3)C$$

$$\frac{dC}{dt} = +k_1 ES - (k_2 + k_3)C$$

$$\frac{dP}{dt} = k_3 C$$

$$\frac{dS}{dt} = -k_3 C$$

The system eventually reaches a quasi-steady-state in which the rates of change of E and C are zero. If E_0 is the total amount of available enzyme (i.e., $E_0 = E + C$), then it is possible to substitute the term ($E_0 - C$) for E.

$$\frac{dP}{dt} = \frac{k_3 E_0 S}{S + (k_2 + k_3)/k_1}$$

The theoretical maximum value for dP/dt is termed v_{max} and occurs when all of the available enzyme is in the bound form (i.e., when $C = E_0$), which would occur when substrate concentrations are very high (at saturation levels). Substituting v_{max} for k_3E_0 and the standard notation k_M for the term $(k_2+k_3)/k_1$ in the above equation yields the hyperbolic, quasi steady-state relationship described by Briggs and Haldane (1925):

$$\frac{dP}{dt} = \frac{v_{max} S}{S + k_M}$$

Note that k_M represents the substrate concentration necessary to achieve a rate of product formation of $v_{max}/2$. k_M also represents the relative affinity of the enzyme for the substrate; higher values of k_M indicate lower affinity. The total amount of enzyme and the enzyme activity (and hence the values v_{max} and k_M) are not necessarily constant over time. Finally, it should be noted that Michaelis and Menton (1913) describe a hyperbolic relationship that is identical to the preceeding equation. However, the underlying assumptions and the definition of k_M differ slightly from the Briggs/Haldane model.

The original Briggs/Haldane model applies to single-substrate reactions. Many metabolic reactions involve more than one substrate. To accommodate multiple substrates, it is necessary to redefine v_{max} as the maximum rate of product production when all substrates are at saturation levels and $k_{M,i}$ as the concentration of substrate S_i at which the rate of product production is $v_{max}/2$ (all other substrates are at saturation levels). It is then possible to derive the following equation for multiple substrates (Indge and Childs, 1976):

$$\frac{dP}{dt} = \frac{v_{max} \prod_{i=1}^{n}[S_i]}{\frac{k_{M1} \prod_{i=1}^{n}[S_i]}{[S_1]} + \frac{k_{M2} \prod_{i=1}^{n}[S_i]}{[S_2]} + .. + \frac{k_{Mn} \prod_{i=1}^{n}[S_i]}{[S_n]} + \prod_{i=1}^{n}[S_i]}$$

where Π represents the mathematical product (multiplication) operator. This equation is formatted similarly to the equation for one substrate. The following form, obtained by dividing numerator and denominator by $\Pi[S_i]$, is more convenient for computational purposes:

$$\frac{dP}{dt} = \frac{v_{max}}{\frac{k_{M1}}{[S_1]} + \frac{k_{M2}}{[S_2]} + .. + \frac{k_{Mn}}{[S_n]} + 1}$$

Maximal, Substrate-Limited Models

In some cases, the reaction rate of a pathway is much faster than other pathways in the model. These pathways tend to be substrate-limited. Systems that include this type of pathway require small time steps in the numerical solution because of the discontinuity around the point of zero substrate concentration and the large rate of product formation when substrate concentrations are non-zero.

To prevent numerical instability at larger time steps, we assume that the rate of conversion of substrate to product (dP/dt) is the same as the rate at which substrate becomes available to the process (dS_{avail}/dt), up to some maximal rate, v_{max}.

$$\frac{dS}{dt} = \begin{cases} \frac{dS_{avail}}{dt} & for \quad \frac{dS_{avail}}{dt} \le v_{max} \\ v_{max} & for \quad \frac{dS_{avail}}{dt} > v_{max} \end{cases}$$

Enzyme Regulation

Enzymes catalyzing rate-determining steps tend to be highly regulated. Activation (A) and inhibition (I) factors may include substrate and product concentrations, other local factors (e.g, amount of available ATP or Ca^{2+}), and centrally produced regulatory factors (e.g., insulin, glucagon, or epinephrine). Regulatory factors may affect enzyme activity levels (k or v_{max}), substrate binding (k_M), or both.

The following equations are used to account for enzyme regulation in the model:

$$k = k_0 \cdot \left(1 + \frac{A}{sf_A} - \frac{I}{sf_I}\right)$$

$$v_{max} = v_{max,0} \cdot \left(1 + \frac{A}{sf_A} - \frac{I}{sf_I}\right)$$

$$k_M = k_{M,0} \cdot \left(1 - \frac{A}{sf_A} + \frac{I}{sf_I}\right)$$

Accounting Procedures

To determine the quantity of a metabolic substance within the model, rates of accumulation of the substance attributed to each connecting pathway are added together. Note that negative rates of accumulation represent a loss. As an example, consider the pathway diagram in Figure 3:

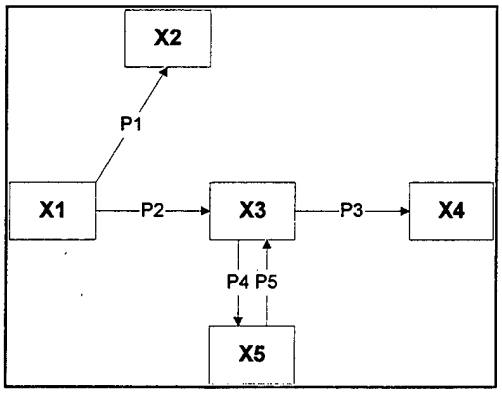

Figure 3 - Generic Pathway Diagram

The substance X1 can be converted to X2, or to X4 or X5 via an intermediate product, X3. The reaction between X3 and X5 is reversible, but uses different mechanisms for the synthesis and degradation of X5. A reaction model and a set of differential equations are generated for each pathway (P1-P5), as described in the preceding subsection. Rates of accumulation of each substance, attributed to each pathway, are added together. The resulting differential equations are solved numerically to obtain the quantity of the substance over time.

For example, for X3:

$$\frac{dX3_{tot}}{dt} = \frac{dX3_{P2}}{dt} + \frac{dX3_{P3}}{dt} + \frac{dX3_{P4}}{dt} + \frac{dX3_{P5}}{dt}$$

$$X3 = \int_0 \frac{dX3_{tot}}{dt}$$

Numerical differential equation solvers, provided within the simulation development environment, are currently used to solve differential equations within DYNUMO.

CENTRAL BLOOD COMPARTMENT

The Central Blood Compartment communicates with all other submodels within DYNUMO. Nutrients are absorbed into the Central Blood Compartment from the Digestive System. The Adipose Tissue submodel takes up fatty acids and glucose from the blood, and releases fatty acids and glycerol into the blood. The Liver Tissue submodel takes up glucose from the blood and stores it as glycogen, for later release as glucose. The Liver Tissue submodel takes up other nutrients, which it converts into glucose for release back into the Central Blood Compartment. Glucose may be taken up from the Central Blood Compartment by Metabolically-Active Tissue and stored as glycogen or used for energy. The Metabolically-Active Tissue also takes up fatty acids for energy use. The Regulatory System senses the glucose level within the blood and modifies levels of insulin and glucagon accordingly.

The only metabolic reaction that takes place within the Central Blood compartment at present is the conversion of triacylglyerol (TriG), incorporated within chylomicrons (see 'Digestive System'), to fatty acids (FA) and glycerol in the blood. Metabolic reactions that occur in connection with other submodels are described under those subheadings. For example, glucose uptake by the liver is described in the section titled 'Liver Tissue.'

Initial Conditions

Volume and Mass

Two volumes are used to describe the Central Blood compartment, the total blood volume and the plasma volume. Plasma volume is computed assuming 0.05L per kg body weight (Shepherd and Vanhoutte, 1979, p. 328). This amounts to 3.5L for a 70 kg man. Blood Volume (V_{blood}) is computed from V_{plasma} assuming a hematocrit value of 42%. This amounts to 6.0 L for a 70 kg man. Central Blood Compartment weight is not used in any computations and is omitted here.

Concentrations

Initial concentrations for each of the substances considered in the Central Blood Compartment model are provided in Table 2 on the following page. Concentrations are given per volume of blood.

Table 2 - Initial Concentrations-Central Blood Compartment

Symbol	Description	Initial Value (*mM)	Reference
G_{blood}	Blood Glucose	4.4	Stryer (1995, p.774)
FA_{blood}	Blood Fatty Acid	0.363	derived
La_{blood}	Blood Lactate	1.0	Newsholme and Leech, 1983, p. 372
AA_{blood}	Blood Amino Acid	1.0	derived
KB_{blood}	Blood Ketone Body	0.1	Newsholme and Leech, 1983, p.282
$Glycerol_{blood}$	Blood Glycerol	0.04	Newsholme and Leech, 1983, p. 372
Insulin	Blood Insulin	14 (μU/ml)	Newsholme and Leech, 1983, p. 372
Glucagon	Blood Glucagon	80 (pg/ml)	Newsholme and Leech, 1983, p. 372
Epinephrine	Blood Epinephrine	0.1 (ng/ml)	Newsholme and Leech, 1983, p. 372
Norepinephrine	Blood Norepinephrine	0.4 (ng/ml)	Newsholme and Leech, 1983, p. 372
$TriG_{CM}$	Triacylglycerol as Chylomicrons	0	
$TriG_{VLDL}$	Triacylglycerol as VLDL	0	

*Unless otherwise noted

Initial values assume a healthy, rested, well-fed individual. Plasma FA concentration is derived so that the resting FA uptake by Metabolically-Active Tissue is equal to 0.4072, which meets requirements for resting metabolism when the respiratory quotient is 0.82 (see 'Metabolically-Active Tissue' section). The value for amino acids is the sum of the values for alanine and glutamine, provided in Newsholme and Leech (1983, p.539).

TriG Conversion to FA and Glycerol in Blood

Neither chylomicrons nor lipoproteins can be taken up directly by a cell. Instead, they are progressively broken down into fatty acids and glycerol, plus smaller "remnant" molecules. Fatty acids and glycerol are removed gradually as the lipoproteins circulate through tissues containing active lipoprotein lipase. Under normal conditions, most of this hydrolysis occurs in the adipose tissue (Newsholme and Leech, 1983, p. 258).

The half-life of chylomicrons in the blood (τ_{CM}) is only four-five minutes (Brown and Goldstein, 1979; Brown et al., 1981). The half-life of VLDL that originates in liver tissue (τ_{VLDL}) is 1-3 hours. (Brown et al., 1981). Using $k = \ln(2)/\tau$, it is possible to compute mass action rate coefficients for the breakdown of chylomicron ($k_{CM} = 0.154$) and VLDL ($k_{VLDL} = 0.00578$) to FA and glycerol in blood. Table 3 summarizes the model for this reaction.

Table 3 - Model Description: TriG Conversion to FA in Blood

Kinetic Model	$TriG_{CM} + CholesterolEster \xrightarrow{k_{CM}} 3FA + \mathrm{Re}mnant$ $TriG_{VLDL} + CholesterolEster \xrightarrow{k_{VLDL}} 3FA + IDL$
Model	*Mass Action*
Mathematical Equations	$\frac{dTriG_{CM}}{dt} = -k_{CM}[TriG_{CM}]$ $\frac{dTriG_{VLDL}}{dt} = -k_{VLDL}[TriG_{VLDL}]$ $\frac{dFA}{dt} = -3\left(\frac{dTriG_{CM}}{dt} + \frac{dTriG_{VLDL}}{dt}\right)$
Parameters k_{CM} (mmol·min^{-1}·mM^{-1}) k_{VLDL} (mmol·min^{-1}·mM^{-1})	0.154 *0.00578*

DIGESTIVE SYSTEM

The Digestive System submodel includes the processes of ingestion, gastric emptying, digestion and absorption of fats and carbohydrates. Protein ingestion and gastric emptying are also included. However, protein digestion and absorption are not considered at this time.

Digestive System Inputs & Outputs

Digestive system inputs include the total volume of ingested food ($V_{ingested}$), the amounts of ingested carbohydrate, fat, and protein ($C_{ingested}$, $F_{ingested}$, and $P_{ingested}$, respectively), and the type of carbohydrate (e.g., simple sugar, starch, or legume). Dietary fiber is not considered at this time. Outputs include the rates and amounts of glucose and triacylglycerol (in the form of chylomicrons) entering the blood compartment.

Ingestion

The ingestion process assumes that food is consumed as a bolus. It updates the volume ($V_{gastric}$) and the amounts of carbohydrate ($C_{gastric}$), fat ($F_{gastric}$), and protein ($P_{gastric}$) in the stomach accordingly:

$$V_{gastric} = V_{gastric} + V_{ingested}$$

$$C_{gastric} = C_{gastric} + C_{ingested}$$

$$F_{gastric} = F_{gastric} + F_{ingested}$$

$$P_{gastric} = P_{gastric} + P_{ingested}$$

Gastric Emptying

Food entering the stomach is assumed to mix with existing stomach contents before passing into the small intestine. The rate of change of gastric volume due to gastric emptying ($dV_{gastric,GE}/dt$) is generally represented by an exponential function (Costil, 1990; George, 1968; Griffith et al., 1968; Harvey et al., 1970; Hunt and Spurrell, 1951; Hunt and Stubbs, 1975; Rehrer et al., 1989; Tinker et al., 1970):

$$\frac{dV_{gastric,GE}}{dt} = -\alpha V_{gastric}$$

Carbohydrate, lipid and protein emptying are assumed to occur by bulk flow:

$$\frac{dC_{gastric,GE}}{dt} = \frac{C_{gastric}}{V_{gastric}} \cdot \frac{dV_{gastric,GE}}{dt}$$

$$\frac{dF_{gastric,GE}}{dt} = \frac{F_{gastric}}{V_{gastric}} \cdot \frac{dV_{gastric,GE}}{dt}$$

$$\frac{dP_{gastric,GE}}{dt} = \frac{P_{gastric}}{V_{gastric}} \cdot \frac{dV_{gastric,GE}}{dt}$$

where $dC_{gastric,GE}/dt$, $dF_{gastric,GE}/dt$ and $dP_{gastric,GE}/dt$ are the rates of change of gastric carbohydrate, fat and protein, respectively, due to gastric emptying. Numerous studies have shown that the rate of gastric emptying slows in proportion to the osmolality of the gastric contents (Barker et al., 1974 and 1978; Brener et al., 1983; Costil and Saltin, 1974; Coyle et al., 1978; Fortran and Ingelfinger, 1968; Foster et al., 1980; Hunt, 1961; Hunt and Knox, 1968; McHugh and Moran, 1979; Moran and McHugh, 1981). However, other studies show no difference in the gastric emptying rates of monosaccaride and polysaccaride solutions of equal concentration (Hunt, 1960; Elias et al., 1968; Foster et al., 1980). Other investigators have hypothesized that the rate of gastric emptying is controlled by the rate of energy delivery to the small intestine (Brener et al., 1983; Costill and Saltin, 1974; Hunt and Stubbs, 1975; McHugh and Moran, 1979; Moran and McHugh, 1981). Using this assumption, Hunt and Stubbs (1975) developed the following relationship using data from 33 different experiments:

$$t_{1/2} = V_0(0.1797 - 0.1670e^{-K})$$

where $t_{1/2}$ is the half-life of the exponential function, V_0 is the initial gastric volume, and K is the caloric density of the gastric contents (assuming 4 kcal/g for carbohydrate and protein, and 9 kcal/g for lipids). By definition, α is equivalent to $\ln(2)/ t_{1/2}$ so that the relationship may be rewritten in terms of the exponential rate coefficient α:

$$\alpha = \frac{\ln(2)}{V_0(0.1797 - 0.1670e^{-K})}$$

Substituting this expression for α into the exponential gastric emptying function, above, yields the following set of equations:

$$\frac{dV_{gastric,GE}}{dt} = -\frac{\ln(2)}{V_{gastric,0}(0.1797 - 0.1670e^{-K})} \cdot V_{gastric}$$

$$\frac{dC_{gastricGE}}{dt} = -\frac{\ln(2)}{V_{gastric,0}(0.1797 - 0.1670e^{-K})} \cdot C_{gastric}$$

$$\frac{dF_{gastricGE}}{dt} = -\frac{\ln(2)}{V_{gastric,0}(0.1797 - 0.1670e^{-K})} \cdot F_{gastric}$$

$$\frac{dP_{gastricGE}}{dt} = -\frac{\ln(2)}{V_{gastric,0}(0.1797 - 0.1670e^{-K})} \cdot P_{gastric}$$

Carbohydrate Digestion & Absorption

Carbohydrate digestion includes those processes involved in the breakdown and transport of carbohydrates in the digestive system. The products of digestion include the monosaccharides glucose, fructose, and galactose. For simplification, all final products of carbohydrate digestion in this model are assumed to be glucose (i.e., all ingested carbohydrates are assumed to be converted to glucose). We assume that the rate of digestion depends on the type or complexity of the carbohydrate, i.e., that starches and legumes take longer to digest than do the mono- and disaccharides. It is not clear whether any of the steps in the digestion process are enzyme-limited. Because

intermediate products are transported away or absorbed, it is unlikely that the process is product-limited.

Absorption of glucose involves transport into the intestinal epithelial cell, then entry into the capillaries. Transport occurs by an active mechanism using the sodium pump and may occur against a concentration gradient. Monosaccharide absorption may also occur by bulk flow through the paracellular pathway (Fordtran, 1975; Gisolfi et al., 1995; Pappenheimer and Reiss, 1987). The paracellular pathway is not considered here.

Although digestion and absorption are clearly two separate processes, the data used to develop and to test the model cannot distinguish between them. Thus, they are considered together here in a single model. Assuming the simplest case, that the processes of digestion and absorption are neither enzyme- nor product-limited, a pipeline model may be used (see Model Overview section). Both the number of segments in the pipeline (n) and the rate coefficient (k) vary according to the type and complexity of the carbohydrate. The variable R in the model is the rate that substrate leaves the stomach. The first substrate in the pipeline, S_0, represents the carbohydrate as it exits the stomach. The product, P, represents the glucose as it passes into the blood.

Parameter estimation for this model was difficult. Experiments using a segmental perfusion technique (Duchman et al., 1997; Gisolfi et al., 1995; Shi et al., 1995; Schedl et al., 1994) provide accurate measurements of water and solute absorption only over a short segment of small intestine. Results cannot be extrapolated to the entire small intestine and are only appropriate during steady state. General results from these studies are still useful, however. Experiments by Duchman et al. (1997), Gisolfi et al. (1995), Shi et al. (1995), and Schedl et al. (1994) show that after an equilibration period, total carbohydrate absorption matches the rate of carbohydrate emptying from the stomach up to rates of approximately 1.8 g/min. The study by Shi et al. (1995) demonstrates that glucose and fructose use parallel absorption pathways, operating independently at approximately the same rate.

The only other data that were immediately available for parameter estimation included measurements of the blood glucose and insulin responses to various carbohydrate meals (Thomas et al., 1991; Taub et al., 1998). These data incorporated not only the digestion and absorption processes, but the gastric emptying and cellular uptake processes as well. In the study conducted by Thomas and coworkers (1991), subjects consumed lentils, potatoes, or glucose (1 gram of available CHO per kg of body mass) plus water, making the total volume of the meal 400 ml. The blood glucose and insulin responses to each meal were measured at 15-minute intervals for one hour. These data were used first to obtain the parameter (η) describing the insulin response to changes in blood glucose (see 'Regulatory System'):

$$Insulin_N = \left(G_{blood,N} - 1\right) \cdot \eta + 1$$

Using these data, η was found to be approximately 3.4. We assumed that resting glucose uptake was 1.04 mmol/min (see Metabolically-Active Tissue section), and that this value would increase with $Insulin_N$ by a proportionality coefficient (ξ). The model parameters

ξ, k, and n were then adjusted to fit the data. Because of the relatively few data points, formal optimization was not performed and adjustments were limited to one significant digit. The values of ξ, k, and n appearing in Table 4 were found to fit the data satisfactorily:

Table 4 - Values of Carbohydrate Digestion & Absorption Model Parameters

CHO Source	*n*	*k*	ξ
Glucose	6	0.6	2.9
Potato (Starch)	6	0.4	2.5
Lentils (Legume)	8	0.4	5.7

Figures 4-6, below, show the predicted and observed blood glucose response to each of the three meals using parameter values in Table 4.

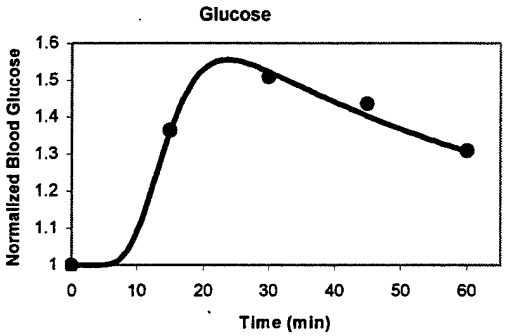

Figure 4 - Predicted (solid line) and Observed (filled circle, mean of eight subjects) Blood Glucose Response To Glucose Ingestion (data from Thomas et al., 1991)

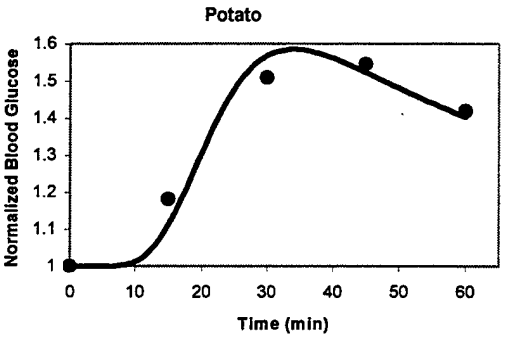

Figure 5 - Predicted (solid line)and Observed (filled circle, mean of eight subjects) Blood Glucose Response To Ingestion Of Potatoes (data from Thomas et al., 1991)

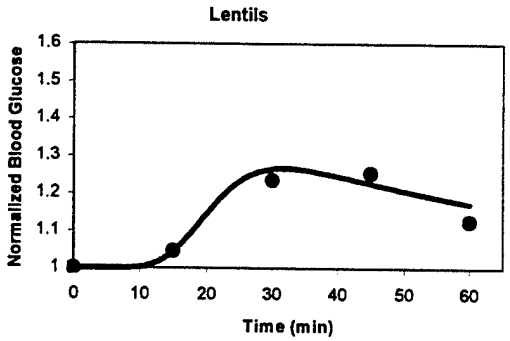

Figure 6 - Predicted (solid line) and Observed (filled circle, mean of eight subjects) Blood Glucose Response To Ingestion Of Lentils

The results of the parameter fitting indicate that foods of high and low glycemic index require different parameter values to accurately represent the digestion and absorption processes. This agrees with other evidence from Crapo et al. (1976) and Jenkins et al. (1991), in which digestion of legumes was slower than that of potato. It should be noted that gastric emptying may be slower for legumes as well (Torsdotti et al. 1984), which is not accounted for in this model. An unexpected result from the fitting procedure was that the relationship between insulin and blood glucose was different for lentils than for glucose or potatoes, which is reflected in the different value for ξ found during the fitting process. The reason for this difference is not known.

A summary of the model for carbohydrate digestion and absorption is provided in Table 5, below.

Table 5 - Model Description: Carbohydrate Digestion and Absorption

Kinetic Equation	$S_0 \xrightarrow{\beta} S_1 \xrightarrow{\beta} S_2 \ldots S_n \xrightarrow{\beta} G$
Model	*Pipeline Model*
Mathematical Equation	$\frac{dS_0}{dt} = -\frac{dC_{gastric}}{dt} - \beta S_0$ $\frac{dS_i}{dt} = \beta(S_{i-1} - S_i), \quad 1 \le i \le n$ $\frac{dG}{dt} = +k_n S_n$
Parameter Values	*see Table 4*

Lipid Digestion & Absorption

Lipid digestion includes those processes involved in the breakdown and transport of fats and lipids in the digestive system. The products of digestion are fatty acids, monoglycerides, lysophophoglycerols, bile acids, phosphate, choline, and cholesterol esters. These products are absorbed by passive diffusion, mainly in the upper half of the small intestine. After entry into the intestinal mucosa, triacylglycerols, phospholipids and cholesterol esters are resynthesized, packaged with small amounts of protein, and then

secreted as chylomicrons into the extracellular space. The chylomicrons move from the extracellular space into the lymphatic system and from there into the subclavian vein. Short chain fatty acids are bound with albumin and released directly into the portal vein. A small amount of very low density lipoprotein (VLDL) and high density lipoprotein (HDL) are also released from the intestine mucosa. For simplification, this model keeps track only of the triacylglycerol packaged within the chylomicron as it enters the blood.

Model details are provided in Table 6 below. The same assumptions and kinetic models are used as for carbohydrate digestion and absorption. Chylomicrons are released into the blood for many hours following a meal heavy in fat content (Linder, 1994). Values of n = 6 and k = 0.05 were arbitrarily selected such that following ingestion of 25 g of fat without cellular uptake by Metabolically-Active Tissue, the rate of absorption peaks at approximately 3 hours and continues through approximately 6 hours. This slow rate of digestion and absorption means that ingested lipids will affect the overall, daily caloric balance, but will not greatly effect activities occurring within a few hours after ingestion.

The model does not currently distinguish among fats of different types or complexities.

Table 6 - Model Description: Lipid Digestion and Absorption

Kinetic Equation	$S_0 \xrightarrow{\beta} S_1 \xrightarrow{\beta} S_2 \ldots S_n \xrightarrow{\beta} TriG$
Model	*Pipeline Model*
Mathematical Equation	$\frac{dS_0}{dt} = -\frac{dF_{gastric}}{dt} - \beta S_0$ $\frac{dS_i}{dt} = \beta(S_{i-1} - S_i), \quad 1 \le i \le n$ $\frac{dTriG}{dt} = +k_n S_n$
Parameter Values β (min^{-1}) n	 *0.05* *6*

Testing

Gastric Emptying

To test the model for gastric emptying, we attempted to simulate the results of five studies found in the literature (Duchman et al., 1997; Rehrer et al., 1992; Seiple et al., 1983; Sole and Noakes, 1989; Vist and Maughan, 1994). These studies included both single ingestion and repeated ingestion (i.e., ingestion at 10- or 20-minute intervals) experiments, carbohydrate concentrations between 0 and 17 g/dl, and both glucose and polymerized glucose solutions. Some solutions included electrolytes, and others did not. The range of ingestion volumes was from 400 ml to 1227 ml. We were unable to find suitable data for gastric emptying of lipid or mixed meals.

In all experiments, the Hunt and Stubbs (1975) model overestimated the rate of gastric emptying for water and underestimated the rate of gastric emptying for carbohydrate

solutions. Errors were reasonable for single ingestion experiments, but relatively large for repeated ingestion experiments. Typical plots of gastric volume over time for single- and for repeated- ingestion experiments are shown in Figure 7 and Figure 8. Observed and predicted values for all simulations are provided in Table 7 on page 26.

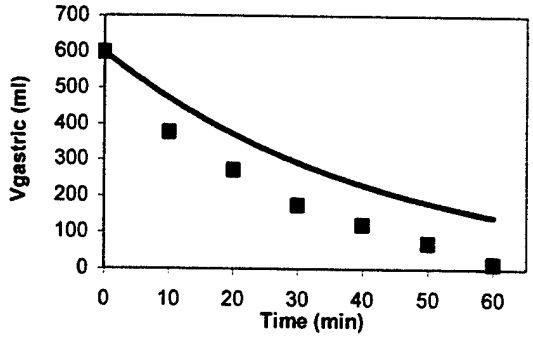

Figure 7 - Predicted (solid line) and Observed (filled square, mean of six subjects) Values Of Gastric Volume Following Single Ingestion Of 600 Ml Of 6% Glucose Solution (data from Vist and Maughan, 1994)

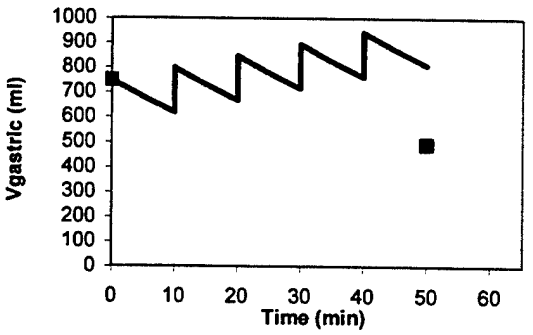

Figure 8 - Predicted (solid line) and Observed (filled square, mean of six subjects) Values Of Gastric Volume Following Single Ingestion Of 750 Ml Of 6% Glucose Solution, Followed By Repeated Ingestion Of 180 Ml Of 6% Glucose Solution At 10-Minute Intervals (data from Duchman et al., 1997)

Digestion & Absorption

To test the model for digestion and absorption, we attempted to simulate the results from two experiments by Taub et al. (1998). In these experiments, subjects ingested a 500 ml, 12% carbohydrate solution. Blood glucose was then recorded over 4 hours. In the first experiment, subjects ingested 12% glucose. In the second experiment, they ingested 12% maltodextrin. Figure 9 and Figure 10 show observed and predicted values for these two experiments when the parameter values given in Table 4 (for glucose) were used in generating the predictions. Although maltodextria is slightly more complex than glucose, its digestion and absorption dynamics are very similar.

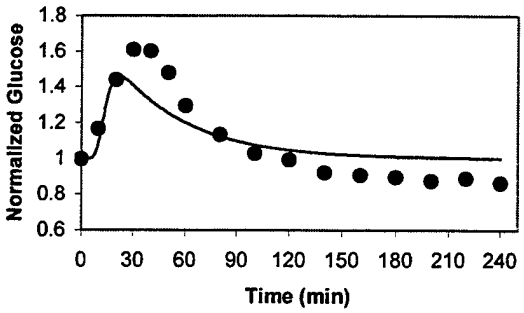

Figure 9 - Predicted (solid line using n=6, k = 0.6, x = 2.9) and Observed (filled circle, mean of five subjects) Blood Glucose Response To Ingestion Of 12% Glucose Solution (data from Taub et al., 1998)

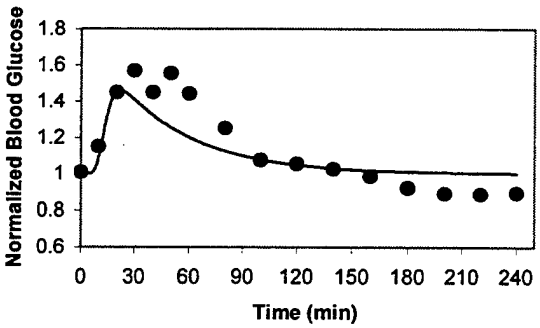

Figure 10 - Predicted (solid line using n=6, k = 0.6, x = 2.9) and Observed (filled circle, mean of six subjects) Blood Glucose Response To Ingestion Of 12% Maltodextrin (data from Taub et al., 1998)

Using parameter values from Table 4, the model underestimates the blood glucose response to ingestion of 12% carbohydrate solution. A slightly better estimate is obtained by changing ξ to 2.0. The results of changing the value for ξ is shown in Figures 11-12.

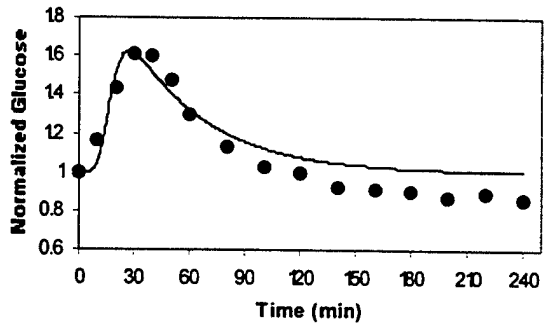

Figure 11 -Predicted (solid line using n=6, k = 0.6, x = 2.0) and Observed (filled circle, mean of five subjects), Blood Glucose Response To Ingestion Of 12% Glucose Solution (data from Taub et al., 1998)

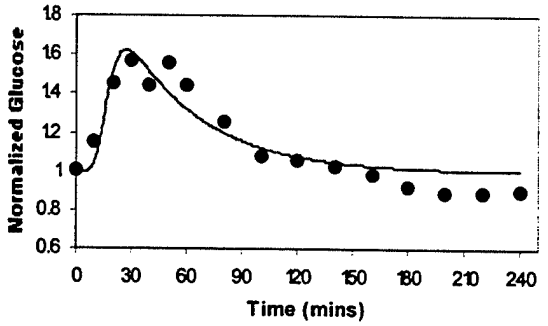

Figure 12 - Predicted (solid line using n=6, k = 0.6, x = 2.0) and Observed (filled circle, mean of six subjects) Blood Glucose Response To Ingestion Of 12% Maltodextrin (data from Taub et al., 1998)

Discussion

The digestive system model presented here represents a first approximation. Neither robust parameter estimation nor thorough model validation were possible with the data obtained to date. The testing conducted thus far is encouraging, but further testing needs to be performed before we can be confident in the predictions.

The model for gastric emptying in particular requires further development. The Hunt and Stubbs model (1975) was used to describe gastric emptying. This model was based on data from 33 different experiments. However, for most of these experiments, the exponential half-life was derived from measurements at only a single time point. Furthermore, this model does not account for observed differences in gastric emptying for solutions of the same caloric density but different osmolality. Model testing showed small but consistent errors in $V_{gastric}$ for single ingestion experiments, and large errors for repeated ingestion experiments. Additional data may be used to obtain better parameter values for the Hunt and Stubbs model (1975), or a different model may be used altogether.

Obtaining a good model of gastric emptying is important because gastric emptying is the primary limiting factor for digestion and absorption (Duchman et al., 1997; Schedl et al., 1994; Shi et al., 1995). When gastric emptying occurs at a constant rate, the digestion/absorption rate will reach the rate of gastric emptying after an equilibration period. The pipeline model used in DYNUMO to describe digestion and absorption simulates this phenomenon well. Again however, parameter value estimation was developed on a very limited data set consisting primarily of glucose ingestion data. No data were available for lipid nutrients. Quantitative effects of dietary fiber, hydration, and electrolytes on digestion and absorption have not yet been included either. Because of these limitations, we recommend that the model be used only for simulation of glucose ingestion at this time. A more intensive data search and parameter value refinement needs to be conducted to extend the validity of the model to include other carbohydrates, fats, and meals consisting of a mixture of nutrients.

Protein digestion and absorption are not considered at this time. Protein digestion and absorption are relatively unimportant for short-term studies or long-term studies when caloric intake is adequate. Changes in the rate of protein metabolism during periods of inadequate nutrition may be considered in future versions of DYNUMO, in which case the dynamics of protein digestion and absorption may need to be implemented as well.

Digestive System model limitations are summarized below:

1. Parameter value estimation was based on a very limited data set (mostly glucose solutions, mostly single ingestion).
2. Protein digestion and absorption dynamics are not considered.
3. Effects of hydration, dietary fiber, and electrolytes on digestion and absorption are not considered.
4. All ingested nutrients are eventually absorbed; no nutrients are lost in the feces.
5. Limits on rates of absorption (Duchman et al., 1997) have not been implemented.
6. Ingested carbohydrates and lipids are assumed to be absorbed as glucose and triacylglycerol; digestion of carbohydrates and lipids to disaccharide, fructose or other lipid (e.g., cholesterol, fatty acid, VLDL, and HLDL) products are not considered.
7. The model does not include effects of exercise or physical activity on gastric emptying, digestion, or absorption.

Table 7 -Observed and Predicted Values for Model of Gastric Emptying

					$V_{gastric}$			
Exp	*Nutrients*	*Conc (%)*	*Time (min)*	$V_{ingested}$ *(ml)*	*Observed (ml)*	*Predicted (ml)*	*Error (ml)*	*Reference*
1	Water Only	0	0	600	600	600		Vist & Maughan, 1994
			10		312	240.6	-71.4	
			20		135	96.5	-38.5	
			30		44	38.7	-5.3	
			40		22	15.5	-6.5	
			50		9	6.2	-2.8	
			60		2	2.5	0.5	
2	Glucose	2	0	600	600	600		Vist & Maughan, 1994
			10		256	381.3	125.3	
			20		128	242.3	114.3	
			30		61	154	93	
			40		37	97.9	60.9	
			50		22	62.2	40.2	
			60		13	39.5	26.5	
3	Glucose	4	0	600	600	600		Vist & Maughan, 1994
			10		360	440.3	80.3	
			20		247	323.1	76.1	
			30		145	237.1	92.1	
			40		90	174	84	
			50		55	127.7	72.7	
			60		29	93.7	64.7	
4	Glucose	6	0	600	600	600		Vist & Maughan, 1994
			10		378	472.3	94.3	
			20		273	371.8	98.8	
			30		176	292.7	116.7	
			40		121	230.4	109.4	
			50		71	181.3	110.3	
			60		14	142.8	128.8	
5	Water Only	0	0	400	400	400		Sole & Noakes, 1989
			15		100†	50.9	-49.1	
6	Glucose	5	0	400	400	400		Sole & Noakes, 1989
			15		185†	218.2	33.2	
7	Glucose	10	0	400	400	400		Sole & Noakes, 1989
			15		275†	272.4	-2.6	
8	Glucose	15	0	400	400	400		Sole & Noakes, 1989
			15		315†	297.7	-17.3	
9	Poly-5-Glucose	5	0	400	400	400		Sole & Noakes, 1989
			15		150†	218.2	68.2	
10	Poly-5-Glucose	10	0	400	400	400		Sole & Noakes, 1989
			15		230†	272.4	42.4	
11	Poly-5-Glucose	15	0	400	400	400		Sole & Noakes, 1989
			15		250†	297.7	47.7	
12	Fructose	5	0	400	400	400		Sole & Noakes, 1989
			15		195†	218.2	23.2	
13	Fructose	10	0	400	400	400		Sole & Noakes, 1989
			15		205†	272.4	67.4	

Table 7 Cont'd

					$V_{gastric}$			
Exp	*Nutrients*	*Conc (%)*	*Time (min)*	$V_{ingested}$ *(ml)*	*Observed (ml)*	*Predicted (ml)*	*Exp*	*Nutrients*
14	Fructose	15	0	400	400	400		Sole & Noakes, 1989
			15		260†	297.7	37.7	
15	Water Only	0	0	400	400	400		Seiple et al., 1983
			30		22.1	6.5	-15.6	
			60		9	0.1	-8.9	
16	PolyGlucose	3	0	400	400	400		Seiple et al., 1983
	Fructose	2	30		40.2	119	78.8	
			60		15.2	35.4	20.2	
17	PolyGlucose	5	0	400	400	400		Seiple et al., 1983
	Fructose	2	30		41.9	151.1	109.2	
			60		12.7	57.1	44.4	
18	Glucose	6	0	750	750	750		Duchman et al., 1997
			10	180				
			20	180				
			30	180				
			40	180				
			50		490	810.2	320.2	
19	Water Only	0	0	608.8	608.8	608.8		Rehrer et al., 1992
			20	228.3				
			40	228.3				
			60	228.3				
			80		36.7	1.92	-34.78	
20	Glucose	4.5	0	608.8	608.8	608.8		Rehrer et al., 1992
			20	228.3				
			40	228.3				
			60	228.3				
			80		70.7	263.7	193	
21	Glucose	17	0	608.8	608.8	608.8		Rehrer et al., 1992
			20	228.3				
			40	228.3				
			60	228.3				
			80		512.7	764.2	251.5	
22	Maltodextrin	17	0	608.8	608.8	608.8		Rehrer et al., 1992
			20	228.3				
			40	228.3				
			60	228.3				
			80		429.7	764.2	334.5	

†Approximate values from Figure 1 in Sole and Noakes (1989).

METABOLICALLY-ACTIVE TISSUE

Metabolically-active tissue includes all the cells in the body that use metabolic fuels to produce ATP to perform physiological work (e.g., muscle contraction, active transport, biosynthesis). Muscle makes up the greatest percentage of metabolically-active tissue by weight, and is responsible for nearly all of the energy consumption that occurs during physical activity. Therefore, we used muscle characteristics to represent the metabolically-active tissue compartment. Pathways within the metabolically-active tissue compartment include glucose metabolism, fatty acid metabolism, and the pathways common to both (Figure 13). Amino acid and ketone body metabolism are not currently included. For simplicity, we consider only the energy transfer between ATP and ADP; guanosine and cytidine nucleoside phosphates (e.g., GTP and CTP) are assumed to be interchangeable with ATP. Also, two adenosine monophosphate (AMP) molecules are considered interchangeable with one ADP.

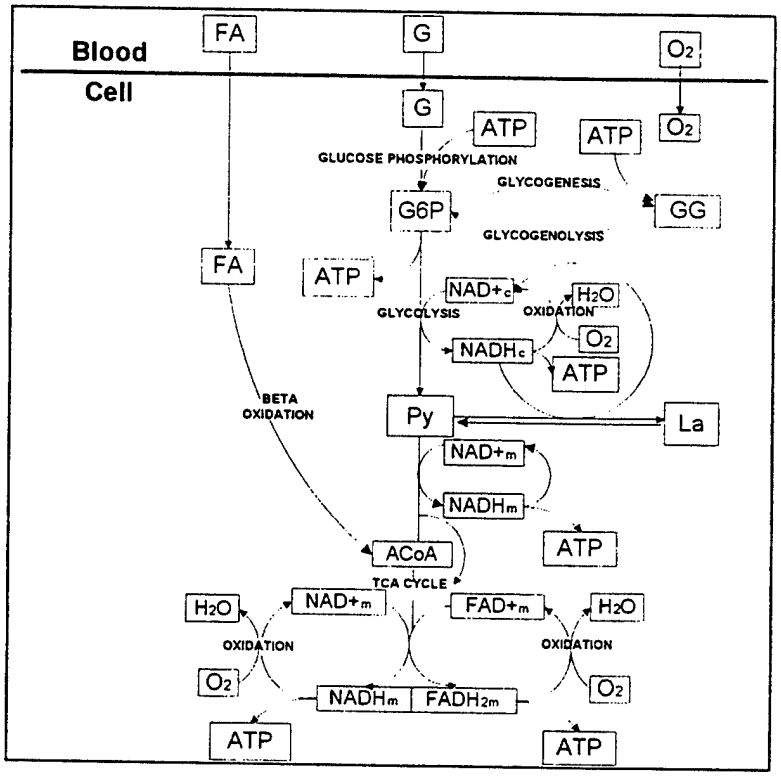

Figure 13 - Model Schematic: Membrane Transport And Metabolic Pathways In The Metabolically-Active Tissue Submodel (definitions of acronyms appear in Table 8)

Initial Conditions

Volume and Mass

Volume of the metabolically-active tissue compartment (V_{cell}) is set to 0.4 L per kg body

weight (Shepherd and Vanhoutte, 1979, p. 328). This amounts to 28 liters for a 70 kg man. Compartment weight was set to 58% of total body weight, which is 100% minus the percentages of body fat (15%), extracellular fluid (20%) and mineral (7%) (Shepherd and Vanhoutte, 1979, p. 328) in the body. This amounts to 40.6 kg for a 70 kg man.

Concentrations

Initial values for each of the substances considered in the model are provided in Table 8.

Table 8 - Initial Concentrations – Metabolically-Active Tissue Model

Symbol	Description	Initial Value (mM)	Reference
$G_{cell,}$	Cellular Glucose	0.1	Newsholme and Leech, 1983, p. 178
G6P	Glucose-6-Phosphate	0.35	Newsholme and Leech, 1983, p. 360
Py	Pyruvate	0.06	Newsholme and Leech, 1983, p. 314
CoA	Coenzyme A	0.05	Newsholme and Leech, 1983, p. 320
ACoA	Acetyl Coenzyme A	0.1	Newsholme and Leech, 1983, p. 110
$NADc^+$	Cytosolic Nicotinamide Adenine Dinucleotide	0.2	derived
$NADH_c$	Cytosolic Nicotinamide Adenine Dinucleotide (reduced form)	0.0002	derived
NAD_m^+	Mitochondrial Nicotinamide Adenine Dinucleotide	0.6	derived
$NADH_m$	Mitochondrial Nicotinamide Adenine Dinucleotide (reduced)	0.075	derived
FAD	Flavin Adenine Dinucleotide	0.2	derived
$FADH_{2,}$	Flavin Adenine Dinucleotide (reduced form)	0.025	derived
ATP	Adenosine Triphosphate	4.0	Stryer, 1995, p. 448
ADP	Adenosine Diphosphate	0.01	Stryer, 1995, p. 448
GG	Glucose Stored As Glycogen	59.52	Newsholme and Leech, 1983, p. 591
FA_{cell}	Cellular Fatty Acid	0.001	derived
La_{cell}	Cellular Lactate	1.0	Newsholme and Leech, 1983, p. 314

Initial values assume a healthy, rested, well-fed individual. Values of cytosolic (subscript c) and mitochondrial (subscript m) NAD^+ and NADH were calculated so that the total amount of NAD^+ in the cell is 0.8 mmol/kg (Newsholme and Leech, 1983, p. 199) and the ratio of NAD^+ to NADH is approximately 1000 in the cytosol and 8 in the mitochondria (Newsholme and Leech, 1983, p. 202). No information could be found regarding the amount of cytosolic versus mitochondrial NAD^+ or NADH substances. It was assumed that the ratio of mitochondrial to cytosolic NADH is 6:2, which is the same as the ratio of mitochondrial to cytosolic NADH production from carbohydrate metabolism under quasi-steady-state conditions. No data were found concerning FAD and $FADH_2$ concentrations. FAD and $FADH_2$ values were set to one sixth of NAD_m^+ and $NADH_m$ values, which is the amount of $FADH_2$ produced during glucose metabolism relative to the amount of NADH produced. No values for CoA were found in the literature. The value of 0.05 is the average of values found for locust flight muscle and

for perfused rat heart (Newsholme and Leech, 1983, p. 321). Similarly, little information was found with respect to human Py concentration. The value of 0.06 mmol/kg is the value for locust flight muscle and for perfused rat heart (Newsholme and Leech, 1983, p. 321) and is slightly greater than the value of 0.03 found for rat kidney (Newsholme and Leech, 1983, p. 524). The value of 0.001 mM for cellular fatty acid was computed assuming that $[FA_{cell}]$ is less than or equal to the fatty acid concentration in true solution (i.e., not bound to protein) in the extracellular space, which is less than 10^{-3} mM. The amount of glycogen in muscle is approximately 300g (Newsholme and Leech, 1983, p. 591). Because the size and weight of the glycogen molecule can vary significantly, we define glycogen in terms of glucose units and the amount of glycogen as the amount of glucose stored as glycogen. Assuming that all 300g of glycogen are available for degradation to glucose, there are 1667 mmol of glucose (MW = 180) stored as glycogen. Using values of V_{cell} and M_{cell} for a 70 kg man, the potential concentration for glucose stored as glycogen is 59.52 mM or 41.06 mmol/kg.

Notation

Throughout this section, amounts of substrate are designated by the symbols shown in the leftmost column of Table 8 Substrate concentrations are designated by these symbols, enclosed in square brackets. For example, the amount of adenosine triphosphate is given by the symbol ATP, while the concentration of ATP is given by [ATP]. Initial amounts or concentrations are designated by the subscript init. Normalized values are denoted by the subscript N, and are computed by dividing a substrate amount or concentration by its initial amount or concentration. For example, ATP_N is computed as ATP/ATP_{init}.

Resting Rates of Metabolic Fuel Consumption

Resting rates of metabolic fuel consumption also assume a healthy, rested, well-fed individual. Resting metabolic rate (MetRate) is approximately 100 kcal/hr. The rate of carbon dioxide that is generated during metabolism divided by the rate of oxygen that is consumed is known as the respiratory quotient (RQ) and it can be used to determine the rate of carbohydrate metabolism relative to fat metabolism. The basal RQ value is 0.82 (Consolazio et al., 1963). The following relationships were used to compute resting rates of glucose and fatty acid metabolism:

$$MetRate = K_G \frac{dG}{dt} + K_{FA} \frac{dFA}{dt}$$

$$RQ = \frac{RQ_G O2_G \frac{dG}{dt} + RQ_{FA} O2_{FA} \frac{dFA}{dt}}{O2_G \frac{dG}{dt} + O2_{FA} \frac{dFA}{dt}}$$

where K is the amount of energy (kcal/hr) and O2 is the amount of oxygen produced per mmol of glucose (subscript G) or fatty acid (subscript FA). Note that these relationships ignore protein metabolism. Solving these equations for dG/dt and dFA/dt yields:

$$\frac{dG}{dt} = \frac{MetRate \cdot O2_{FA}(RQ - RQ_{FA})}{K_G O2_{FA}(RQ - RQ_{FA}) + K_{FA} O2_G (RQ_G - RQ)}$$

$$\frac{dFA}{dt} = \frac{MetRate \cdot O2_G (RQ_G - RQ)}{K_G O2_{FA}(RQ - RQ_{FA}) + K_{FA} O2_G (RQ_G - RQ)}$$

Substituting values from Table 9 on the following page, the resting rate of glucose consumption $(dG/dt)_{init}$ is 1.0406 mmol/min and the resting rate of fatty acid consumption $(dFA/dt)_{init}$ is 0.4072 mmol/min.

Table 9 - Metabolic Parameter Values

Fuel	*K (kcal per mmol)*	*O2 (mmol per mmol)*	*RQ*
Glucose (subscript G)	0.686	6	1.0
Fatty Acid (subscript FA)	2.34	23	0.7

Glucose Metabolism

Glucose Uptake

Glucose transport between the blood compartment and Metabolically-Active Tissue is typically far from equilibrium (Newsholme and Leech, 1983, pg. 184). Blood glucose (G_{blood}) concentration is generally higher than cellular (G_{cell}) concentration. This is due in large part to glucose phosphorylation (see next subsection), which irreversibly transforms cellular glucose into glucose-6-phosphate. However, when glucose phosphorylation is inhibited, glucose may accumulate in the cell and approach equilibrium with the blood. Therefore, a bi-directional uptake/release model is used.

Glucose transport across the cell membrane occurs via facilitated diffusion, in which glucose is transported passively across the cell membrane using one or more of a family of transport molecules (GLUT1-GLUT5). Since the amount of carrier is limited, the Quasi-Steady-State Saturation Kinetic model (see Model Overview section) is used to describe this pathway. GLUT2 and GLUT5 are present in liver, intestinal, and pancreatic cells and are not considered in this section. GLUT1 and GLUT3 are responsible for basal glucose uptake. The k_M for GLUT1 and GLUT3 is typically around 1.0 mM, much lower than the normal serum glucose level, which is typically 4.0 – 8.0 mM (Stryer, 1995, p.505). GLUT4 has a k_m of approximately 5.0 mM (Stryer, 1995, p.505) and mediates the entry of glucose into muscle and adipose cells.. The number of GLUT4 transporters increases markedly in the presence of insulin (Stryer, 1995, p.505) and physical training (Houmard et al., 1993). Glucose uptake increases during skeletal muscle contraction (Richter et al., 1986) increasing up to 7-20 times basal levels during exercise and remaining 3-4 times the basal level for 40 minutes after exercise, despite normal lactate and VO2 levels (Wahren et al., 1973). This effect occurs both in the presence of insulin (Berger et al., 1975), and in the absence of insulin (Wahren et al., 1971), with the combined effect of skeletal muscle contractions and insulin being additive (Ploug et al.,

1984, 1985). Although epinephrine and norepinephrine have been shown to decrease glucose uptake, this is more likely an indirect effect of increased FA mobilization than a direct effect on glucose uptake (Wasserman and Vranic, 1986).

The model for glucose uptake is described in Table 10. The terms $f_{insulin}$ and $f_{contraction}$ are used to represent the effects of insulin and muscular contraction on glucose uptake. $f_{insulin}$ and $f_{contraction}$ take on values between 0 to 1, where 0 represents no effect and 1 represents maximal effect. $f_{insulin}$ is computed from $Insulin_N$ ($f_{insulin} = (Insulin_N - 1)/10$), while $f_{contraction}$ is currently input by the user. Model parameter values were computed assuming that glucose uptake equals $(dG/dt)_{init}$ when $f_{insulin} = 0$ and $f_{contraction} = 0$, glucose uptake equals $10 \cdot (dG/dt)_{init}$ when $f_{insulin} = 1$or $f_{contraction} = 1$. k_M was assumed to be 1.0 when $f_{insulin}$ and $f_{contraction}$ equal zero, and 5.0 when $f_{insulin}=1$ or $f_{contraction}=1$. Values for v_{max} were computed using values of $[G_{blood}]_{init}$ and $[G_{cell}]_{init}$ and the assumed values of glucose uptake and k_M described above. The effects of $f_{insulin}$ and $f_{contraction}$ were assumed to be additive. The value for v_{max} at $f_{contraction}=0$ and $f_{insulin}=0$ is 1.4 mmol/min/kg, which is close to the value of 1.167 mmol/min/kg found by Morgan et al. (1961) for perfused rat hindquarters in the absence of insulin.

Table 10 - Model Description: Glucose Uptake

Kinetic Equation	$G_{blood} \xleftarrow{carrier} G_{cell}$
Model	*Quasi-Steady-State Saturation Kinetic model*
Mathematical Equations	$\frac{dG_{cell}}{dt} = \frac{v_{max}}{\frac{k_M}{[G_{blood}]}+1} - \frac{v_{max}}{\frac{k_M}{[G_{cell}]}+1}$ $\frac{dG_{blood}}{dt} = -\frac{dG_{cell}}{dt}$
Regulation of k_M (mM)	
$k_{M,0}$	*1.0*
Inhibition Term	$f_{insulin} + f_{contraction}$
Scaling Factor	*0.025*
Regulation of v_{max} (mmol/kg min)	
$v_{max,0}$	*1.4016*
Activation Term	$f_{insulin} + f_{contraction}$
Scaling Factor	*0.0692*

Glucose Phosphorylation

Once glucose enters Metabolically-Active Tissue, it is irreversibly bound to a phosphate group. The resulting molecule, glucose-6-phosphate (G6P) cannot be transported back across the cell membrane, so glucose is effectively captured in the cell by its binding with phosphate. One molecule of ATP is required for each molecule of glucose that is phosphorylated. Glucose phosphorylation is catalyzed by hexokinase, which is inhibited by its product, G6P (Newsholme and Leech, 1983, p. 184, Stryer, 1995, p. 495). High concentrations of G6P cause changes in the hexokinase molecule that decrease its affinity for glucose (increase its k_M value). We were unable to find quantitative relationships between [G6P] and changes in k_M in the literature. For the time being, we assume the

enzyme is inhibited when $[G6P]_N$=1 and is uninhibited when $[G6P]_N$ =0.5. At normal [G6P] levels, we assume that the rate of glucose phosphorylation is $(dG/dt)_{init}$ and that the k_M value is 0.1 mM (Newsholme and Leech, 1983, p. 178; Stryer, 1995, p.495). v_{max} is set to 1.0 mmol/min/kg, which is the value given for muscle hexokinase in fit subjects (Newsholme and Leech, 1983, p.369).

Solving for sf_I yields the results presented in Table 11. The kinetic model comes from Stryer (1995, p. 491).

Table 11 - Model Description: Glucose Phosphorylation

Kinetic Model	$G_{cell} + ATP \xrightarrow{hexokinase} G6P + ADP + H^+$
Model	*Quasi-Steady-State Saturation Kinetic model*
Mathematical Equations	$\frac{dG6P}{dt} = v_{max} \cdot \frac{1}{\frac{k_M}{[G_{cell}]} + 1}, [ATP] > 0$ $\frac{dG_{cell}}{dt} = -\frac{dG6P}{dt}$ $\frac{dATP}{dt} = -\frac{dG6P}{dt}$
v_{max} (mmol/kg min)	*1.0*
Regulation of k_M (mM)	
$k_{M,0}$	*0.1*
Inhibition Term	$[G6P]_N$-*0.5*
Scaling Factor (Inhibition)	*0.02*

Glycolysis

Glycolysis is typically defined as the process of splitting one molecule of glucose into 2 molecules of pyruvate. Because of the need to keep track of G6P levels, in DYNUMO, glycolysis starts with G6P and ends with the formation of two pyruvate molecules. Four molecules of ATP are produced and one molecule of ATP is consumed for each G6P molecule consumed during glycolysis.

Glycolysis includes several metabolic reactions. The rate-determining step is catalyzed by 6-phosphofructokinase (6PFK). High levels of ATP lower the affinity of 6PFK for its substrate, while high levels of substrate stimulate 6PFK (Stryer, 1995, p.493-495). Citrate enhances the inhibitory effect of ATP (Stryer, 1995, p. 494) and helps regulate glucose metabolism relative to fatty acid metabolism.

Pyruvate kinase also partially controls glycolysis. Glucagon, which is increased when blood glucose is low, lowers pyruvate kinase activity (Stryer, 1995, p. 496),thereby restricting use of glucose when carbohydrates are in short supply. Like 6PFK, Pyruvate kinase is inhibited by ATP and excited by ADP. Pyruvate kinase is also inhibited by phosphocreatine (PCr), which explains the preferential use of PCr when it is available.

In DYNUMO, glycolysis is assumed to be inhibited by high levels of ATP. Control via citrate is ignored. Instead, control of glucose vs. fat metabolism is accomplished at the

next step, conversion of pyruvate into ACoA, which is inhibited by its end product, ACoA. Control by glucagon is also ignored for the present, accomplished in part by insulin regulation of glucose uptake. Although control via Ca^{2+} or epinephrine is not explicitly stated, we know that the enzyme is capable of a wide range of activity, enabling glycolysis to achieve rates ranging from nearly zero during carbohydrate depletion to maximal rates of 2000 mmol/min or higher during maximal, all-out efforts. Rapid changes in the rate of glycolysis is achieved through feedforward control by MetRate (presumably through Ca^{2+} or epinephrine), with fine control achieved through inhibition by ATP. This approach enables glycolysis to keep pace with glycogen degradation, which is controlled to a great extent by epinephrine levels. Alternative approaches, including increasing the sensitivity to substrate concentrations or increasing the gain on the ATP inhibition mechanism, tend to lead to numerical instability. The interaction between glycolysis and PCr metabolism is not included in the current model.

Table 12 provides a model description of the glycolysis pathway. The resting rate of pyruvate generation via glycolysis is set to $2\cdot(dG/dt)_{init}$. v_{max} is set to three times the rate of glucose utilization that is required for anaerobic, glucose-only metabolism for a given metabolic rate. The rate of pyruvate generation via glycolysis is set to 90% of v_{max} when $[ATP]_N$=0.5. k_M is computed assuming [G6P] =$[G6P]_{init}$. The kinetic model comes from Stryer (1995, p. 491).

Table 12 - Model Description: Glycolysis

Kinetic Model	$G6P + 3ADP + 2NAD^+ + 2Pi \xrightarrow{6PFK} 2Py + 3ATP + 2NADH + H^+ + 2H_2O$
Model	*Quasi-Steady-State Saturation Kinetic model*
Mathematical Equations	$\frac{dPy}{dt} = \frac{v_{max}}{\frac{k_{M,G6P}}{[G6P]} + 1}, [NAD^+] > 0, [ADP] > 0$ $\frac{dG6P}{dt} = -\frac{1}{2}\cdot\frac{dPy}{dt}$ $\frac{dADP}{dt} = -\frac{3}{2}\cdot\frac{dPy}{dt}$ $\frac{dNADH}{dt} = +\frac{dPy}{dt}$
Regulation of v_{max} (mmol/min) $v_{max,0}$ (mmol/kg min) Activation Term Scaling Factor (Activation)	 171.233 *MetRate-75* *75*
Regulation of $k_{M,G6P}$ (mM) $k_{M,0}$ Inhibition Term Scaling Factor (Inhibition)	 *0.0389* *$[ATP]_N$-0.5* *0.00051*

AcoA from Pyruvate

Pyruvate Dehydrogenase (PD) catalyzes the first step in the metabolic pathway that starts with pyruvate and ends with the formation of acetyl coenzyme A (ACoA). PD likely

catalyzes the rate-determining step (Newsholme and Leech, 1983, p.192). PD is a three-enzyme complex which is regulated via phosphorylation (inactivation) and dephosphorylation (activation). In essence, PD is acticated by Py and Ca^{2+}, and is inhibited by high levels of ATP, ACoA and NAD^+.

Table 13 provides a detailed description of the Py-to-ACoA pathway. The simplified regulatory scheme used in DYNUMO assumes that the enzyme is activated by muscular contraction (Ca^{2+}) and inhibited by ACoA. Activation by Ca^{2+} is accomplished by making v_{max} a function of MetRate. The resting rate of ACoA production is set to $2 \cdot (dG/dt)_{init}$. The factor of two is necessary because 2 moles of Py are produced for every mole of G consumed. v_{max} is set to the rate required for glucose-only metabolism for a given metabolic rate multiplied by 2.5. The rate of ACoA production is assumed to be 80% of v_{max} when $[ACoA]_N$=0.5. k_M is computed assuming [Py] = $[Py]_{init}$. The kinetic model comes from Stryer (1995, p.514).

Table 13 - Model Description: Pyruvate-to-ACoA

Kinetic Model	$CoA + Py + NAD^+ \longrightarrow ACoA + NADH + CO_2$
Model	*Quasi-Steady-State Saturation Kinetic model*
Mathematical Equations	$\frac{dACoA}{dt} = \frac{v_{max}}{\frac{k_{M,Py}}{[Py]} + \frac{k_{M,CoA}}{[CoA]} + 1}, [NAD^+] > 0$ $\frac{dPy}{dt} = \frac{-dACoA}{dt}$ $\frac{dCoA}{dt} = \frac{-dACoA}{dt}$ $\frac{dNAD^+}{dt} = \frac{-dACoA}{dt}$
Regulation of v_{max} (mmol/min) $v_{max,0}$ (mmol/kg min) Activation Term Scaling Factor (Activation)	 4.56 *MetRate-75* *75*
$k_{M,ACoA}$ (mM)	*0.008*
Regulation of $k_{M,Py}$ (mM) $k_{M,0}$ Inhibition Term Scaling Factor (Inhibition)	 *0.00504* *$[ACoA]_N$-0.5* *0.027*

Glycogen Synthesis

Glycogen is synthesized from G6P. For ease in bookkeeping, glycogen is considered to be made up of glucose units; the amount of glycogen is defined as the amount of glucose stored as glycogen. Glycogen synthase catalyzes a non-equilibrium reaction, which is likely the rate-determining step (Newsholme and Leech, 1983, p. 586). Glycogen synthase can exist in many forms with different activation levels (Newsholme and Leech, 1983, p. 591) and is regulated by several factors in a very complex mechanism. Epinephrine and Ca^{2+}, which are increased with exercise or sympathetic activity, reduce

glycogen synthase activity, while high insulin and low glycogen levels increase glycogen synthase activity (Richter et al., 1984; Newsholme and Leech, 1983, p. 591). Replenishment and even supercompensation of glycogen levels are possible only after muscle glycogen has been sufficiently depleted (Bonen et al., 1985; Conlee et al., 1978; Terjung et al., 1974).

For simplification, this model assumes that glycogen synthesis is controlled primarily via product inhibition. It is assumed that v_{max} is zero when muscle glycogen is at normal levels, and that it rises to 28 mmol/min (1 mmol/min/L) when muscle glycogen is completely depleted. The value of 28 mmol/min was selected arbitrarily. k_M was set to a low value such that the rate of synthesis is determined primarily by v_{max}. This regulation scheme accounts for replenishment of glycogen following depletion, but does not account for supercompensation of glycogen observed following carbohydrate depletion/loading regimens. Table 14 provides a detailed description of the glycogen synthesis pathway. The kinetic model is from Stryer (1995, p. 588).

Table 14 - Model Description: Glycogen Synthesis

Kinetic Model	$G6P + ATP + GG_n + H_2O \xrightarrow{GG-synthase} GG_{n+1} + ADP + 2P_i$
Model	*Quasi-Steady-State Saturation Kinetic model*
Mathematical Equations	$\frac{dGG}{dt} = \frac{v_{max}}{\frac{k_M}{[G6P]} + 1}, [ATP] > 0$ $\frac{dG6P}{dt} = -\frac{dGG}{dt}$ $\frac{dATP}{dt} = -\frac{dGG}{dt}$
k_M (mM)	*0.05*
Regulation of v_{max} (mmol/min) $v_{max,0}$ (mmol/min) Inhibition Term Scaling Factor (Inhibition)	 *28* $[GG]_N$ *1*

Glycogen Degradation (Glycogenolysis)

During glycogen degradation, glycogen is broken down using successive phosphorylation to form G6P. Glycogen degradation occurs by a completely different mechanism than glycogen synthesis. Phosphorylase catalyzes the rate-determining step. It removes glucose units sequentially from the outer branches of the glycogen molecule up to about 4 glucose units from the branch point. Phosphorylase used alone would leave about 50% of the glycogen molecule intact; branching enzymes are used to split the molecule further. For simplification, the activity of the branching enzyme is considered coincident with that of phosphorylase.

During rest, phosphorylase is inactive (~99% in inactive muscle) so that glycogen can be stored (Guyton, 1977, p. 709). Phosphorylase is regulated via interconversion cycles by factors related to energy metabolism (Newsholme and Leech, 1983, p. 198). It is activated by Ca^{2+}, epinephrine and glucagon (Newsholme and Leech, 1983, p. 325).

AMP, IMP, and Pi increase while ATP and G6P decrease the activity of the inactive form of phosphorylase.

Table 15 provides a detailed description of the glycogenolysis pathway used in DYNUMO. The simplified regulatory scheme assumes that the enzyme is activated by Ca^{2+} and epinephrine. This is implemented by making v_{max} a function of MetRate. We also assume fine control via ATP inhibition. v_{max} is set to the rate required for glucose-only, anaerobic metabolism for a given metabolic rate multiplied by 2. It is assumed that at rest, when $[G6P]_N$=1, the rate of G6P production via glycogenolysis is approximately zero. It is also assumed that when $[G6P]_N$=0.5 the reaction rate is 90% of v_{max}. The kinetic model comes from Stryer (1995, p.583-585).

Table 15 - Model Description: Glycogenolysis

Kinetic Model	$GG_n + P_i \longrightarrow GG_{n-1} + G6P$
Model	*Quasi-Steady-State Saturation Kinetic model*
Mathematical Equations	$\frac{dG6P}{dt} = \frac{v_{max}}{\frac{k_M}{[GG]}+1}$ $\frac{dGG}{dt} = -\frac{dG6P}{dt}$
Regulation of v_{max} (mmol/min)	
$v_{max,0}$ (mmol/kg min)	114.155
Activation Term	*MetRate-75*
Scaling Factor (Activation)	*75*
Regulation of $k_{M,G6P}$ (mM)	
$k_{M,0}$	*6.6138*
Inhibition Term	$[ATP]_N$*-0.5*
Scaling Factor (Inhibition)	$8.87x10^{-6}$

Pruvate-Lactate Reaction

The end products for glycolysis include pyruvate, NADH, and H^+. Under aerobic conditions, the NADH produced during glycolysis undergoes electron transport and oxidative phosphorylation, producing ATP and converting NADH to NAD^+. This reformation of NAD^+ is critical for glycolysis to continue. Under very high work rates or hypoxic conditions (e.g. high altitude) oxygen may not enter the cell rapidly enough to meet ATP requirements using oxidative metabolism alone. Under these anaerobic conditions, the pyruvate-lactate reaction (see Table 16, p. 38) reduces NADH to NAD^+. At sea level, anaerobic metabolism becomes significant at activity levels of approximately 50-70% of $VO_{2,max}$. At altitude, $VO_{2,max}$ decreases as altitude increases, resulting in lower thresholds (in terms of absolute metabolic rate) for anaerobic metabolism. Lactate dehydrogenase catalyzes the Py-to-La reaction, which is near-equilibrium. Because the reaction is near-equilibrium, the reaction is readily reversible (Newsholme and Leech, 1983, p.206), and enzyme regulation has little effect on the reaction rate as compared to changes in substrate concentration. The rate of lactate release from muscle reaches a peak of approximately 140 mmol/min/100 ml blood within a few minutes of the onset of exercise, then it decreases (Newsholme and Leech, 1983, p.

217, Figure 5.22). 140 mmol/min/100 ml blood is equivalent to approximately 172 mmol/min/kg muscle, assuming a blood volume of 5L and a compartment weight of 40.6 kg. A reaction coefficient, k, derived by assuming that the maximal reaction rate of 172 mmol/min/kg occurs when lactate is at its initial value and pyruvate and NADH are at twice their initial values, is very large. Because the Py-to-La reaction is expected to keep pace with glycolysis, a maximal, substrate-limited model with a maximum rate of 172 mmol/min/kg is used. dPy_{avail}/dt is computed by subtracting the rate of Py conversion to ACoA from the rate of Py production in glycolysis. The kinetic model comes from Stryer (1995, p. 497).

Table 16 - Model Description: Pyruvate-Lactate Reaction

Kinetic Model	$Py + NADH + H^+ \longleftrightarrow La + NAD^+$
Model	*Maximal, Substrate-Limited*
Mathematical Equations	$\frac{dLa}{dt} = \begin{cases} \frac{dPy_{avail}}{dt} & for \quad \frac{dPy_{avail}}{dt} \le v_{max} \\ v_{max} & for \quad \frac{dPy_{avail}}{dt} > v_{max} \end{cases}$ $\frac{dNADH}{dt} = -\frac{dLa}{dt}$ $\frac{dPy}{dt} = -\frac{dLa}{dt}$
v_{max} (mmol/min/kg)	*172*

Lactate Release

Lactate produced in the muscle is rapidly released into the blood. Assuming a diffusion mechanism, the rate is influenced by the blood concentration of lactate, which is influenced by both muscle release and by liver uptake. This agrees with experimental observations of high initial rates of lactate release from muscle (140 mmol/min/100 ml blood) within a few minutes after onset of exercise, then a decrease over time (Newsholme and Leech, 1983, p. 217, Figure 5.22). This also agrees with observations of blood lactate levels reaching 2-20 mM depending on the severity of the work (Wahren et al., 1971; Galbo et al., 1975) and training of the subject (Rennie et al., 1974). We assume that [La] is 1.0 mM in both blood (see Table 2 and muscle and that this value can increase to as high as 20 mM in muscle during severe work. k is computed assuming a maximum diffusion rate of 172 mmol/min/kg when $[La_{cell}]$ is 20 mM and $[La_{blood}]$ is 1.0 mM. The details of the model are provided in Table 17.

Table 17 - Model Description: Lactate Release

Kinetic Model	$La_{cell} \xleftrightarrow{k} La_{blood}$
Model	*Mass Action*
Mathematical Equations	$\frac{dLa_{cell}}{dt} = k([La_{blood}]-[La_{cell}])$ $\frac{dLa_{blood}}{dt} = -\frac{dLa_{cell}}{dt}$
k (mmol/min/kg/mM)	*9.053*

Fatty Acid Metabolism

Long chain fatty acids arise from the hydrolysis of triacylglycerol within adipose tissue and are released into the bloodstream after formation. Fatty acids are not released by any other tissue. FAs are transported in blood by binding with albumin and are oxidized in most tissues.

Fatty Acid Uptake

FA transport into the cells is a passive process (Newsholme and Leech, 1983, p. 264). During both brief and prolonged exercise (Ahlborg et al., 1974), FA uptake is in direct proportion to FA delivery to the tissue. There is no evidence of a carrier molecule or cellular regulation, so a simple diffusion model (i,e., mass action model) is assumed. Entry into the cell occurs only when the fatty acid concentration inside the cell ($[FA_{cell}]$) is less than the fatty acid concentration in true solution (i.e., not bound to protein) in the extracellular space (i.e., $<10^{-3}$ mM). Data from Ahlborg et al. (1974) were used to obtain the value for the diffusion coefficient, k. Human male subjects exercised at approximately 30% of $VO_{2,max}$ for 240 minutes. $[FA_{blood}]$ as well as the percentage of the total metabolic rate accounted for by fatty acid metabolism were collected at 0, 40, 180, and 240 minutes. MetRate was computed to be 460 kcal/hr assuming $VO_{2,max} = 4.4$ l/min. FA uptake (mmol/min) was computed by multiplying MetRate by the fraction of MetRate accounted for by fatty acid metabolism and dividing by the kcal generated per mmol of fatty acid (2.340 kcal/mmol). $[FA_{cell}]$ was assumed constant at its initial value, 0.001 mM.

Linear regression analysis yielded a value for k of 1.122 mmol/min/mM. The details of the model are provided in Table 18, below.

Table 18 - Model Description: Fatty Acid Uptake

Kinetic Model	$FA_{blood} \overset{k}{\longleftrightarrow} FA_{cell}$
Model	*Mass Action*
Mathematical Equations	$\frac{dFA_{cell}}{dt} = k([FA_{blood}]-[FA_{cell}])$ $\frac{dFA_{blood}}{dt} = -\frac{dFA_{cell}}{dt}$
k (mmol/min/mM)	1.122

Fatty Acid Activation and Oxidation

FA's must be "activated" before they can be transported into the mitochondria, where they are oxidized. The activation equation (Stryer, 1995, p. 607) is given below:

$$FA + CoA + ATP + H_2O \longrightarrow aCoA + 2ADP + 2P_i + 2H^+$$

The activated fatty acid, acyl coenzyme A (aCoA) is carried across the mitochondrial membrane by carnitine. Once inside the mitochondria, aCoA is degraded two carbon units at a time by a sequence of four reactions called the β-oxidation sequence. The four reactions are: (1) oxidation linked to FAD, (2) hydration, (3) oxidation linked to NAD+, and (4) thiolysis by CoA. The overall reaction for an n-carbon aCoA (C_n-aCoA) is:

$$C_n aCoA + \left(\frac{n}{2}-1\right)FAD + \left(\frac{n}{2}-1\right)NAD^+ + \left(\frac{n}{2}-1\right)CoA + \left(\frac{n}{2}-1\right)H_2O$$
$$\longrightarrow \left(\frac{n}{2}\right)ACoA + \left(\frac{n}{2}-1\right)FADH_2 + \left(\frac{n}{2}-1\right)NADH + \left(\frac{n}{2}-1\right)H^+$$

Combining the reactions of activation and oxidation yields the following net reaction:

$$FA_n + CoA + 2ATP + \left(\frac{n}{2}-1\right)FAD + \left(\frac{n}{2}-1\right)NAD^+ + \left(\frac{n}{2}-1\right)CoA + \left(\frac{n}{2}-1\right)H_2O$$
$$\longrightarrow 2ADP + 2P_i + \left(\frac{n}{2}\right)ACoA + \left(\frac{n}{2}-1\right)FADH_2 + \left(\frac{n}{2}-1\right)NADH + \left(\frac{n}{2}+1\right)H^+$$

We currently do not have information regarding appropriate pathway models, parameter values, or regulatory mechanisms for FA activation and oxidation. Under normal circumstances, FA metabolism is regulated primarily by the rate of FA mobilization from adipose tissue, not by factors within the cell itself. At this time, we will assume that the activation and oxidation processes happen very rapidly so that the rate-limiting factor is the rate of delivery of substrate to the pathway (dFA_{avail}/dt). v_{max} is computed assuming

that FA oxidation can provide up to 50% of $\dot{V}O_{2,max}$. We also assume a 16-carbon activated fatty acid. Details are provided in Table 19, below. The kinetic model comes from Stryer (1995, p. 610-611).

Table 19 - Model Description: Fatty Acid Activation and Oxidation

Kinetic Model	$FA_{16} + 2ATP + 7FAD + 7NAD^+ + 8CoA + 7H_2O \longrightarrow 2ADP + 2P_i + 8ACoA + 7FADH_2 + 7NADH + 7H^+$
Model	*Maximal, Substrate-Limited*
Mathematical Equations	$\frac{dFA}{dt} = \begin{cases} \frac{dFA_{avail}}{dt} & for \quad \frac{dFA_{avail}}{dt} \le v_{max} \\ v_{max} & for \quad \frac{dFA_{avail}}{dt} > v_{max} \end{cases}$ $\frac{dACoA}{dt} = -8\frac{dFA}{dt}$ $\frac{dFADH_2}{dt} = -7\frac{dFA}{dt}$ $\frac{dNADH}{dt} = -7\frac{dFA}{dt}$ $\frac{dATP}{dt} = +2\frac{dFA}{dt}$ $\frac{dCoA}{dt} = +8\frac{dFA}{dt}$
v_{max} (mmol/min)	*4.27*

Citric Acid Cycle

The citric acid cycle is the common degrative pathway for ATP production for all three types of metabolic fuel (see Figure 14). Glucose and fatty acid metabolism produce ACoA, which combines with oxaloacetate in the citric acid cycle to produce NADH and $FADH_2$.

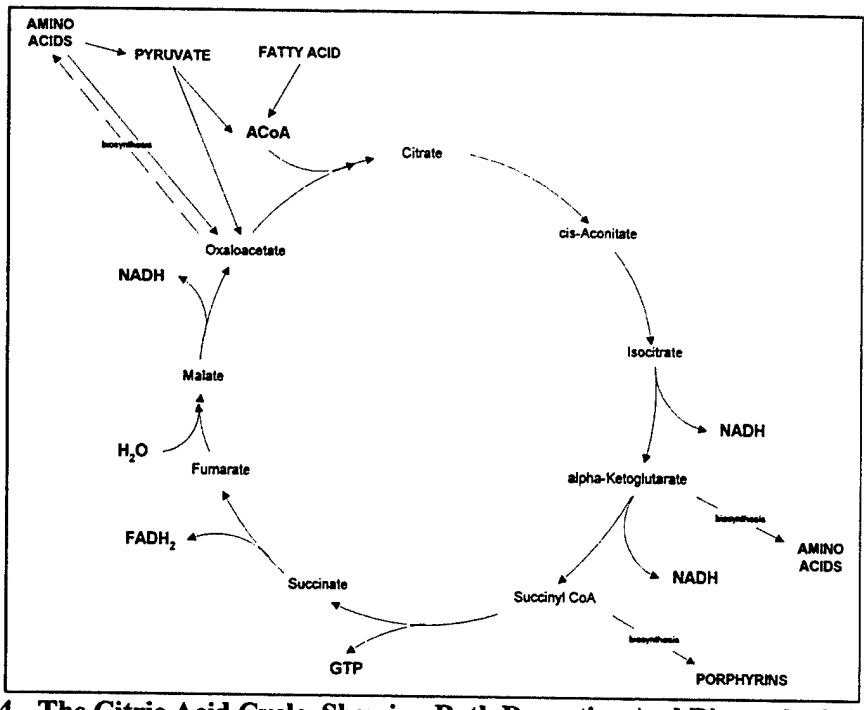

Figure 14 - The Citric Acid Cycle, Showing Both Degrative And Biosynthetic Pathways (from Stryer, 1995, pp. 513, 522)

The rate of the citric acid cycle is precisely regulated to meet ATP requirements (Stryer, 1995, p. 525). Citrate synthase and 2-oxoglutarate dehydrogenase are likely the rate-determining steps. Citrate and ATP inhibit citrate synthase activity (citrate increases the k_M for ACoA) while ATP inhibits and Ca^{2+},[NAD^+]/[NADH] and [CoA]/[succinyl CoA] increase activity of 2-oxoglutarate dehydrogenase. Isocitrate dehydrogenase is a third control point, which is stimulated by Ca^{2+}, and NAD^+, and inhibited by NADH (Newsholme and Leech, 1983, p.320). The common regulatory theme is that high levels of ATP and citrate inhibit the cycle, while Ca^{2+} ADP, NAD^+ and CoA increase enzyme activity. According to Newsholme and Leech (1983, p. 323), Ca^{2+} is the most important regulator. This is accomplished in the model by making v_{max} a function of MetRate. Regulation by ATP/ADP is also important. In DYNUMO, k_M is a function of ATP_N, enabling the reaction rate to be fine-tuned to meet ATP requirements.

Table 20 provides a detailed description of the citric acid cycle. The kinetic model is from Stryer (1995, p. 513). Parameter values were computed assuming a reaction rate of 4.86 mmol/min, which is the rate required for glucose-only metabolism (RQ = 1) at rest. v_{max} is set to the rate required for glucose-only metabolism for a given metabolic rate multiplied by 8.0. It is assumed that the CoA production rate is 50% of v_{max} when $[ATP]_N$=0.5. k_M is computed assuming [ACoA] = $[ACoA]_{init}$.

Table 20 - Model Description: Citric Acid Cycle

Kinetic Models	$ACoA + 2H_2O + 3NAD^+ + FAD + ADP + Pi \longrightarrow 2CO_2 + 3NADH + FADH_2 + CoA + ATP + 2H^+$
Model	*Quasi-Steady-State Saturation Kinetic model*
Mathematical Equations	$\frac{dCoA}{dt} = \frac{v_{max}}{\frac{k_{M,ACoA}}{[ACoA]} + 1}, [NAD^+] > 0, [FAD] > 0, [ADP] > 0$ $\frac{dACoA}{dt} = -\frac{dCoA}{dt}$ $\frac{dNADH_m}{dt} = 3\frac{dCoA}{dt}$ $\frac{dFADH_2}{dt} = \frac{dCoA}{dt}$ $\frac{dATP}{dt} = \frac{dCoA}{dt}$
Regulation of v_{max} (mmol/min)	
$v_{max,0}$ (mmol/kg min)	14.577
Activation Term	*MetRate-75*
Scaling Factor (Activation)	*75*
Regulation of $k_{M,G6P}$ (mM)	
$k_{M,0}$	*0.1*
Inhibition Term	$[ATP]_N$*-0.5*
Scaling Factor (Inhibition)	*0.25*

In addition to its role as a common degrative pathway for ATP production, the citric acid cycle also provides key substrates for biosynthesis (see Figure 4). For example, α-ketoglutarate and oxaloacetate both lead to the biosynthesis of certain amino acids. Neither biosynthesis nor the drawing off of pyruvate to replenish citric acid cycle intermediates is included at this time.

Electron Transport and Oxidative Phosphorylation

Oxidative phosphorylation is the process by which ATP is formed as electrons are transferred from NADH or $FADH_2$ to O_2 by a series of electron carriers in the mitochondrial membrane. NADH and $FADH_2$ are produced during both glucose and fatty acid metabolism. Reactions of electron transport and oxidative phosphorylation appear to be near-equilibrium and thus can be effectively regulated by small changes in substrate concentration (Newsholme and Leech, 1983, p. 324). Several compounds (e.g., cyanide) inhibit electron transfer and therefore prevent oxidative phosphorylation. The rate of oxidative phosphorylation is determined by the rate of ATP hydrolysis (e.g., due to muscle contraction) in the cytosol.

Because NADH and NAD^+ cannot cross the mitochondrial membrane, it is necessary to treat cytosolic (subscript c) separate from mitochondrial (subscript m) NADH and NAD^+. We assume that electron transport and oxidative phosphorylation occur very rapidly in

the presence of $NADH_c$, $NADH_m$, $FADH_2$, and oxygen, and also that the process is limited by substrate availability.

Therefore, we assume that the process keeps pace with NADH and $FADH_2$ production up until the requirement for oxygen ($VO_{2,req}$) exceeds 80% of $VO_{2,max}$, the approximate threshold for aerobic-only metabolism. When $VO_{2,req}$ is less than $VO_{2,max}$, rates of coenzyme reduction and oxidation (redox) are set equal to rates of coenzyme production. When $VO_{2,req}$ is greater than $VO_{2,max}$, on the other hand, rates of coenzyme reduction and oxidation are necessarily limited. We assume that $NADH_c$, $NADH_m$, and $FADH_2$ redox reactions are limited by the same relative amount.

The following reduction/oxidation equations are assumed for NADH and $FADH_2$:

$$NADH + \frac{1}{2}O_2 + H^+ \rightarrow NAD^+ + H_2O$$

$$FADH_2 + \frac{1}{2}O_2 \rightarrow FAD + H_2O$$

The following equation describes ATP synthesis:

$$ADP + P_i + H^+ \rightarrow ATP + H_2O$$

According to Stryer (1995, p. 529-556), electrons are transferred from $NADH_m$ in a three-step process that pumps protons across the inner mitochondrial membrane. The number of protons transported at each of the three steps in the process are 4, 2, and 4 (Stryer, 1995, p.551). It is not exactly clear how the pumping of protons is linked to phosphorylation of ADP to form ATP, but it requires approximately 4 protons to generate a molecule of ATP and to transport it into the cytosol (Stryer, 1995, p.551). Thus, approximately 10 protons are pumped across the mitochondrial membrane and 2.5 moles of ATP are generated as a result of the flow of electrons from $NADH_m$ to O_2. $NADH_c$ and $FADH_2$ enter the pathway at the second step. They pump only 6 protons across the mitochondrial membrane and generate 1.5 moles of ATP per mole of $NADH_c$ or $FADH_2$.

Combining the 2 sets of equations, above, yields the kinetic model, shown in Table 21, below.

Table 21 - Model Description: Electron Transport and Oxidative Phosphorylation

Kinetic Model	$2NADH_c + O_2 + 3ADP + 3Pi + 5H^+ \longrightarrow 2NAD_c^+ + 5H_2O + 3ATP$ $2NADH_m + O_2 + 5ADP + 5Pi + 7H^+ \longrightarrow 2NAD_m^+ + 7H_2O + 5ATP$ $2FADH_2 + O_2 + 3ADP + 3Pi + 3H^+ \longrightarrow 2FAD + 5H_2O + 3ATP$
Model	*Maximal, Substrate-Limited*
Mathematical Equations	$\dot{V}O_{2,req} = 0.5 \cdot \left(\frac{dNADH_c}{dt} + \frac{dNADH_m}{dt} + \frac{dFADH_2}{dt} \right)_{avail}$ $\frac{dATP}{dt} = -\left(1.5\frac{dNADH_c}{dt} + 2.5\frac{dNADH_m}{dt} + 1.5\frac{dFADH_2}{dt} \right)_{redox}$ $\frac{dNADH_c}{dt} = -\begin{cases} \frac{dNADH_{c,avail}}{dt} & for \quad \frac{dNADH_{c,avail}}{dt} \le v_{\max,NADH_c} \\ v_{\max,NADH_c} & for \quad \frac{dNADH_{c,avail}}{dt} > v_{\max,NADH_c} \end{cases}$ $\frac{dNADH_m}{dt} = -\begin{cases} \frac{dNADH_{m,avail}}{dt} & for \quad \frac{dNADH_{m,avail}}{dt} \le v_{\max,NADH_m} \\ v_{\max,NADH_m} & for \quad \frac{dNADH_{m,avail}}{dt} > v_{\max,NADH_m} \end{cases}$ $\frac{dFADH_2}{dt} = -\begin{cases} \frac{dFADH_{2,avail}}{dt} & for \quad \frac{dFADH_{2,avail}}{dt} \le v_{\max,FADH_2} \\ v_{\max,FADH_2} & for \quad \frac{dFADH_{2,avail}}{dt} > v_{\max,FADH_2} \end{cases}$
v_{max} *(mmol/min)*	$v_{\max,NADH_c} = \frac{dNADH_{c,avail}}{dt} \cdot \frac{\dot{V}O_{2,\max}}{\dot{V}O_{2,req}}$ $v_{\max,NADH_m} = \frac{dNADH_{m,avail}}{dt} \cdot \frac{\dot{V}O_{2,\max}}{\dot{V}O_{2,req}}$ $v_{\max,FADH_2} = \frac{dFADH_{2,avail}}{dt} \cdot \frac{\dot{V}O_{2,\max}}{\dot{V}O_{2,req}}$

Testing

Three tests have been designed and conducted thus far. These are intended to test the function of glucose metabolism, fatty acid metabolism, and common metabolic pathways.

Resting State

The objective of this test is to ensure that a system at rest stays at rest. Input conditions for the first test appear in Table 22 as follows:

Table 22 - Model Inputs for Resting Condition

Parameter	*Description*	*Value*
TF	Length Of Experiment (min)	60
StepSize	Step size for Euler solution of differential equations (min)	0.005
VO2max	Maximal Rate of Oxygen Uptake (mmol/min)	196.5
V_{plasma}	Plasma Volume (L)	3.5
$[G_{blood}]$	Blood Glucose Concentration (mM)	5
$[FA_{blood}]$	Free Fatty Acid Concentration In Blood (mM)	0.363
MetRate	Metabolic Rate (kcal/hr)	100
$f_{contraction}$	Muscle Contraction Factor (range 0-1)	0
f_{epi}	Epinephrine Factor (range 0-1)	0
$f_{insulin}$	Insulin Factor (range 0-1)	0
$f_{glucagon}$	Glucagon Factor (range 0-1)	0

Over the 60-minute simulation, substrates neither accumulated nor declined. This was viewed as successful completion and indicated that initial conditions and parameter values were set appropriately for the resting condition.

Submaximal Exercise

The objective of this test is to ensure that the system will arrive at new metabolic fuel consumption rates and will reach a relative steady state with respect to ATP concentration in response to submaximal exercise. It is expected that the system is able to maintain this ATP concentration until metabolic fuels are depleted. Blood glucose and fatty acid concentrations are maintained at constant levels, so that muscle glycogen is the limiting metabolic fuel.

Metabolic rates were set to correspond to 30%, 70%, and 83% of $VO_{2,max}$, given RQ values of 0.82, 0.90, and 0.915, respectively. The blood fatty acid concentration was assumed to be a function of MetRate. Blood glucose was maintained at 5 mM.

A summary of the input conditions for the submaximal exercise simulations appears in Table 23.

Table 23 - Model Inputs for Submaximal Exercise

Parameter	*Description*	*Value*		
		30% of $VO_{2,max}$	70% of $VO_{2,max}$	83% of $VO_{2,max}$
TF	Length Of Experiment (min)	60	60	60
StepSize	Step size for Euler solution of differential equations (min)	0.005	0.005	0.005
VO2max	Maximal Rate of Oxygen Uptake (mmol/min)	196.5	196.5	196.5
V_{plasma}	Plasma Volume (L)	3.5	3.5	3.5
$[G_{blood}]$	Blood Glucose Concentration (mM)	5	5	5
$[FA_{blood}]$	Free Fatty Acid Concentration In Blood (mM)	0.78	1.776	1.789
MetRate	Metabolic Rate (kcal/hr)	315.86	714.71	1117.35
$f_{contraction}$	Muscle Contraction Factor (range 0-1)	1	1	1
f_{epi}	Epinephrine Factor (range 0-1)	1	1	1
$f_{insulin}$	Insulin Factor (range 0-1)	0	0	0
$f_{glucagon}$	Glucagon Factor (range 0-1)	0	0	0
RQ	Respiratory Quotient	0.82	0.90	0.915

Results of these simulations are provided in Figure 15 The system rapidly reached new steady-state values of ATP concentration. Glycogen decreased over time, with the greatest decrease occurring at the highest metabolic rate. Glycogen breakdown responded rapidly to increased ATP production requirements, with glucose uptake responding at a much slower rate.

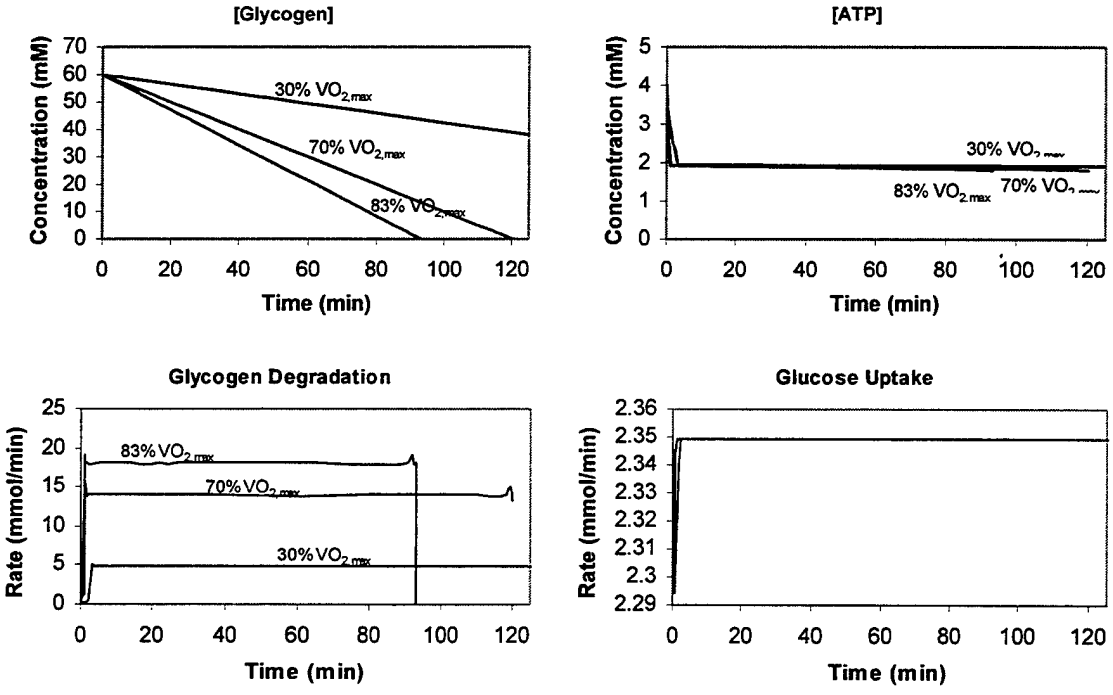

Figure 15 - Model Testing Results For Submaximal Exercise "All-Out" Sprint

The objective of this test is to ensure that the limits placed on the system are appropriate. Aerobic metabolism is necessarily limited by the maximum rate of oxygen uptake. Excess NADH, produced during glycolysis, must be converted to NAD^+ via conversion of pyruvate to lactate. Energy expenditure during a 100m all-out sprint is approximately 200 kJ/min as measured by the staircase method of Margaria et al. (1966). This is equivalent to 3333 Watts or 2866 kcal/hr. Input conditions for the test are summarized in Table 24.

Table 24 - Model Inputs for 'All-Out Sprint'

Parameter	*Description*	*Value*
TF	Length Of Experiment (min)	1
StepSize	Step size for Euler solution of differential equations (min)	0.001
VO2max	Maximal Rate of Oxygen Uptake (mmol/min)	196.5
V_{blood}	Blood Volume (L)	6
$[G_{blood}]$	Blood Glucose Concentration (mM)	5
$[FA_{blood}]$	Free Fatty Acid Concentration In Blood (mM)	0.363
MetRate	Metabolic Rate (kcal/hr)	2866
$f_{contraction}$	Muscle Contraction Factor (range 0-1)	1
f_{epi}	Epinephrine Factor (range 0-1)	1
$f_{insulin}$	Insulin Factor (range 0-1)	0
$f_{glucagon}$	Glucagon Factor (range 0-1)	0

The resulting predictions (Figure 16) agree with the observation that during maximum sprinting, exhaustion occurs at approxiately 20 seconds (Newsholme and Leech, 1983, p. 361), and that at exhaustion, muscle glycogen is greater than half its resting value (Hermansen, 1981).

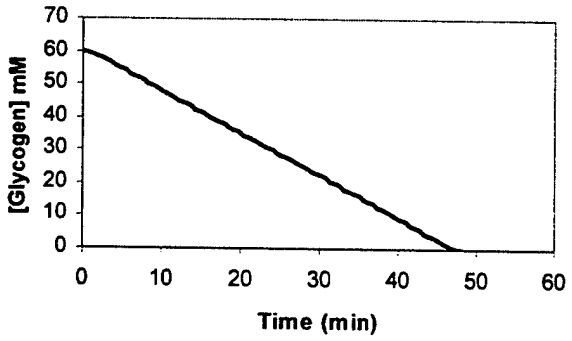

Figure 16 - Model Testing Results For All Out Sprint

Discussion

At present, the Metabolically-Active Tissue model is complete in terms of model coding for carbohydrate and fatty acid energy metabolism. Coding for amino acid and ketone body metabolism remains to be done. Parameter values for fatty acid and carbohydrate metabolism have been derived based on experimental data and on known system behavior. Although a few parameter values were found in the literature, these most often come from in vitro experiments involving single reactions, which may not be applicable to net pathway reactions in vivo.

Ca^{2+} and epinephrine activate several key, rate-controlling enzymes in the processes of glycogen degradation, glycolysis, and the citric acid cycle. This control is implemented in DYNUMO by assuming that Ca^{2+} and epinephrine levels, and hence v_{max} values, are directly related to MetRate. This implementation enables the pathways to respond rapidly to ATP demands associated with physical activity. Raising the v_{max} value at the onset of exercise enables reaction rates to increase quickly to approximately the values necessary for achieving steady-state ATP concentrations. End product inhibition and other local regulatory mechanisms fine-tune the pathway.

A major assumption in the Metabolically-Active Tissue model is that the compartment is represented by skeletal muscle characteristics. Skeletal muscle does not characterize all metabolically-active tissue well. For example, some cells of the body cannot utilize anaerobic metabolic pathways, store glycogen, or utilize fatty acids for fuel. Better resolution may be obtained by separating the Metabolically-Active Tissue compartment into Skeletal Muscle, Brain, and "Other" compartments.

In fact, it may be necessary to further subdivide the Metabolically-Active Tissue compartment by dividing muscle up into several individual compartments. Currently, DYNUMO keeps track of "whole-body" muscle glycogen. However, muscle glycogen cannot leave the cell. If only 20% of the muscle is active, the glycogen in that 20% could be depleted (and the active muscle glycogen exhausted), while the whole-body glycogen level is still at 80%. Unless we wish to determine the glycogen exhaustion threshold separately for each different types of exercise/activity, it would be necessary to track glycogen in active muscle separately from that in inactive muscle. When multiple tasks are considered, for example primarily upper-body work followed by primarily lower-body work, multiple active muscle compartments must be considered.

One limitation of the current model is that the use of metabolic fuels for biosynthesis or to replenish citric acid cycle intermediates used up in the biosynthesis (i.e., anaplerotic reactions) is not considered. The citric acid cycle is not only the source of substrate for aerobic ATP generation; it is also the source of substrate for intermediates of biosynthesis. These intermediates must be replenished if any are drawn off for biosynthesis. During severe carbohydrate depletion, it is possible that without the pyruvate that arises from carbohydrate or amino acid metabolism, citric acid cycle intermediates used for biosynthesis would not be replenished and the citric acid cycle and net fatty acid metabolism would gradually slow down. The implication is that carbohydrate utilization is probably underestimated. The degree of underestimation is probably in the range of 5-20% (Chatham and Phil, 2001).

Another limitation/concern is that throughout, we compute changes in substrate concentration based on organ volume. In many cases, the volume or "space" into which the substance may diffuse is much smaller. Also, we have not considered the interstitial space in this model. With respect to the interstitial space, the parameter values for substrate uptake are based on experimental data in which the interstitial space was implicitly included. With respect to the difference in total organ volume and substrate "space," the use of the entire organ volume likely leads to an underestimation of substrate

concentration changes. Because most of the parameter values were derived based on changes in substrate concentration based on entire organ volume, underestimation of changes in substrate concentration are probably offset by overestimation of reaction rate coefficients.

A thorough validation of the Metabolically-Active Tissue model is required. This should include validation of predictions of the relative contributions of FA and G at various rates of energy expenditure or epinephrine levels. It should also include validation of predictions of the relative contributions of glucose from blood and from glycogen at various energy expenditure levels.

ADIPOSE TISSUE

Adipose tissue cells are the primary storage depots for triacylglycerols (TriG) in the body. Chylomicrons, very low density lipoproteins (VLDL), fatty acids, and glucose in the blood serve as precursors. During high rates of energy expenditure or reductions in carbohydrate stores, adipose cell TriGs are converted to fatty acids (FA) and glycerol, which are released into the blood. Figure 17, below, shows the pathways that are considered in this section.

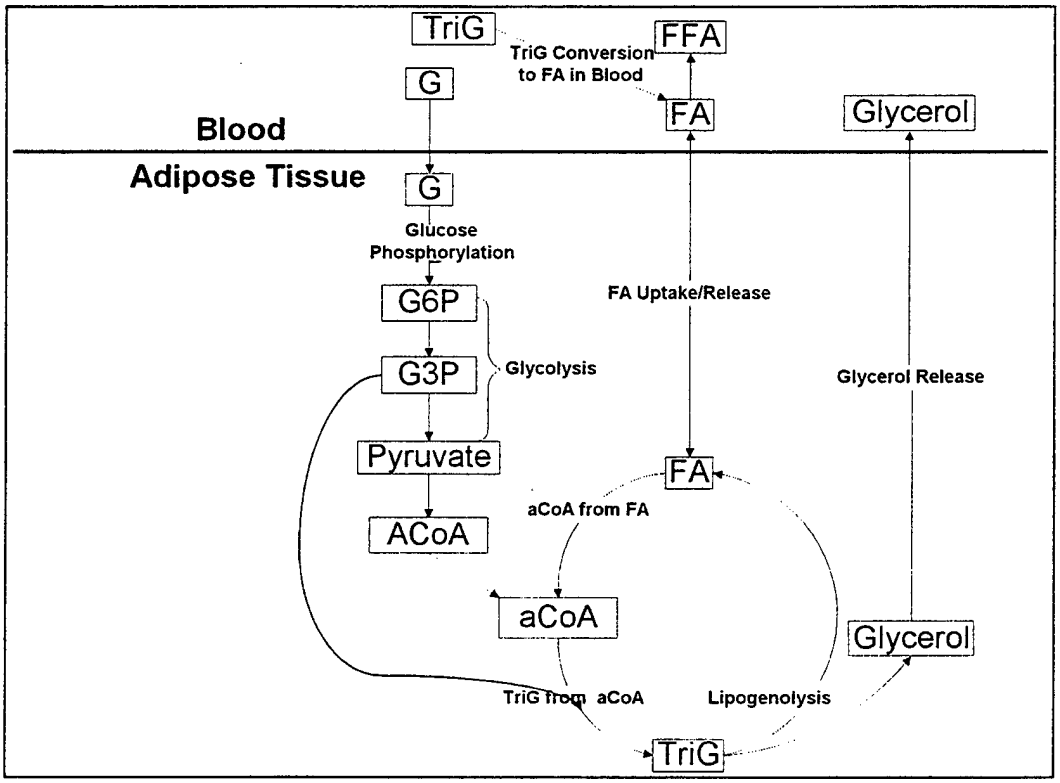

Figure 17 - Model Schematic: Membrane Transport And Metabolic Pathways In The Adipose Tissue Submodel

Neither chylomicrons nor VLDL can pass through the adipose cell membrane. Instead, TriGs are extracted from these larger structures and then broken down into FA and glycerol in the blood (see 'Central Blood Compartment' section). Blood FA, whether from the breakdown of TriGs or in the form of free fatty acids (FFA), diffuses through the adipose cell membrane and enters the adipose cell. Once inside the cell, FAs can diffuse back out of the cell, or can be converted to acyl coenzyme-A (aCoA), which is the precursor for TriG. This series of reactions is described in the subsection 'aCoA from TriG and FA.'

TriG can also be synthesized from glucose. Glucose enters the adipose cell, is phosphorylated, and then participates in the glycolytic pathway in the same way that it does in Metabolically-Active Tissue (see previous section). The pyruvate generated during glycolysis is converted to acetyl coenzyme-A (ACoA). Several ACoA molecules join in an energy-requiring process to form a long chain aCoA molecule, which is the

precursor for TriG. This series of reactions is described in the subsection 'aCoA from Glucose.'

Whether from FA or from glucose precursors, TriG is synthesized by combining three aCoA molecules with one molecule of glyceraldehyde-3-phosphate (G3P), regulated by ACoA carboxylase. The process is the same whether the aCoA was synthesized from glucose, lipid, or fatty acid precursors. This reaction is described in the subsection 'TriG Synthesis.' Note that the G3P used in this reaction is synthesized from G6P during glycolysis. The use of some of the G3P generated during glycolysis to synthesize TriG instead of pyruvate is an important difference between glycolysis in Metabolically-Active Tissue and Adipose Tissue. The use of G3P is also an important regulatory mechanism, ensuring that TriG synthesis does not occur when glucose is in short supply.

The final subsection, 'TriG Degradation' describes the degradation of TriG into FA and glycerol molecules, both of which may be released into the blood.

Although FA and glucose are also used to generate energy for the adipose cells, energy consumption by adipose cells for TriG synthesis is trivial compared to that by the Metabolically-Active Tissue. Therefore, only the triacylglycerol storage and degradation of the adipose cells are considered here.

Initial Conditions

Volume and Mass

Compartment weight was set assuming 15% body fat (Shepherd and Vanhoutte, 1979, p. 328). This amounts to 10.5 kg for a 70 kg man. Assuming a tissue density of 0.9 g/ml for adipose tissue, compartment volume is set to 11.7 L.

Concentrations

Initial values for each of the substances considered in the model are provided below, in Table 25:

Table 25 - Initial Concentrations – Adipose Tissue Model

Symbol	Description	Initial Value (mM)	Reference
$G_{cell,}$	Cellular Glucose	0.1	
FA_{cell}	Cellular Fatty Acid	0.001	derived
TriG	Triacylglycerol	1000	derived
G6P	Glucose-6-Phosphate	0.1	
G3P	Glyceraldehyde-3-Phosphate	0.1	
Py	Pyruvate	0.1	
aCoA	Acyl Coenzyme A	0.1	
CoA	Coenzyme A	0.1	
ACoA	Acetyl Coenzyme A	0.1	
Glycerol	Glycerol	0.1	

Initial values assume a healthy, rested, well-fed individual. The value of 0.001 mM for cellular fatty acid (FA_{cell}) was computed assuming that [FA_{cell}] is less than or equal to the fatty acid concentration in true solution (i.e., not bound to protein) in the extracellular space, which is less than 10^{-3} mM. The value for [TriG] is based on a typical cellular concentration of 0.9 g/g tissue (Newsholme and Leech, 1983, p. 275) or 9.45 kg of TriG

for a 70 kg man (15% body fat). Using a molecular weight of 807 (tripalmitoylglycerol), the milimolar concentration is 1000 mM. The remaining substrate concentrations were arbitrarily set to 0.1 mM for now.

Resting Rates of Substrate Uptake and Product Release
Resting rates of substrate uptake and product release also assume a healthy, rested, well-fed individual. We assume that net glucose uptake is zero under resting conditions when [G_{blood}] is 5 mM. Net glucose uptake will increase as [G_{blood}] and $Insulin_N$ increase. We assume that net FA uptake is zero under resting conditions when [$TriG_{blood}$] is zero. Resting FA release is set to 0.407 mmol/min, which is the rate of consumption of FA by the Metabolically-Active Tissue at rest.

aCoA from TriG and FA

The process of converting FA to aCoA in the Adipose Tissue submodel involves the following processes:

1. Diffusion of FA into and out of the Adipose Tissue, described in subsection 'FA Uptake.'
2. Conversion of cellular FA to aCoA, described in the subsection 'Conversion of FA to aCoA.'

FA Uptake
The transport of FA into adipose cells is a passive process. Currently, there is no evidence of a carrier system (Newsholme and Leech, 1983, p. 261), so we assume it occurs by simple diffusion. The parameter value, k, is the same as that used in the Metabolically-Active Tissue submodel, adjusted for differences in tissue mass. The details of the model are provided in Table 26, below.

Table 26 - Model Description: FA Uptake (Adipose Tissue)

Kinetic Model	$FA_{blood} \overset{k}{\longleftrightarrow} FA_{cell}$
Model	*Mass Action*
Mathematical Equations	$\frac{dFA_{cell}}{dt} = k([FA_{blood}]-[FA_{cell}])$ $\frac{dFA_{blood}}{dt} = -\frac{dFA_{cell}}{dt}$
k (mmol min^{-1} mM^{-1})	*0.29*

Conversion of FA to aCoA
As in the Metabolically-Active Tissue submodel, we assume a maximal, substrate-limited model. The kinetic equation is from Stryer (1995, p. 607).

The details of the model are provided in Table 27.

Table 27 - Model Description: Conversion of FA to aCoA (Adipose Tissue)

Kinetic Model	$FA + CoA + 2ATP + H_2O \longrightarrow aCoA + 2ADP + 2P_i + 2H^+$
Model	*Maximal, Substrate-Limited*
Mathematical Equations	$\frac{daCoA}{dt} = \begin{cases} \frac{dFA_{avail}}{dt} & for \quad \frac{dFA_{avail}}{dt} \le v_{max} \\ v_{max} & for \quad \frac{dFA_{avail}}{dt} > v_{max} \end{cases}$ $\frac{dFA}{dt} = -\frac{daCoA}{dt}$ $\frac{dATP}{dt} = -2 \cdot \frac{daCoA}{dt}$

aCoA from Glucose

Glucose Uptake

Glucose transporters in adipose tissue (GLUT1, GLUT3, and GLUT4) are the same as those in muscle tissue (Stryer, 1995, p. 505). We therefore assume the same kinetic model, mathematical equations, and k_M values as in the Metabolically-Active Tissue. However, we assume essentially zero glucose uptake by adipose tissue at rest, with an increase to 5.0 mmol/min when insulin levels are high. Under these conditions, v_{max} values are different than for Metabolically-Active Tissue. A description of the glucose uptake process is provided in Table 28.

Table 28 - Model Description: Glucose Uptake (Adipose Tissue)

Kinetic Equation	$G_{blood} \xleftarrow{carrier} G_{cell}$
Model	*Quasi-Steady-State Saturation Kinetic model*
Mathematical Equations	$\frac{dG_{cell}}{dt} = \frac{v_{max}}{\frac{k_M}{[G_{blood}]}+1} - \frac{v_{max}}{\frac{k_M}{[G_{cell}]}+1}$ $\frac{dG_{blood}}{dt} = -\frac{dG_{cell}}{dt}$
Regulation of v_{max} (mmol/kg·min) $v_{max,0}$ Activation Term Scaling Factor (Activation)	 *10.408* *$Insulin_N$-1* *10*
Regulation of k_M (mM) $k_{M,0}$ Inhibition Term Scaling Factor (Inhibition)	 *1.0* *$Insulin_N$-1* *0.25*

Glucose Phosphorylation

Glucose phosphorylation is assumed to occur in the same way as in the Metabolically-Active Tissue. Parameter values have not been adjusted at this time. Therefore, the reaction rate will approach 1 mmol/min as $[G_{cell}]$ approaches 0.1 mM. Table 29 describes the model for glucose phosphorylation in adipose tissue.

Table 29 - Model Description: Glucose Phosphorylation (Adipose Tissue)

Kinetic Model	$G_{cell} + ATP \xrightarrow{hexokinase} G6P + ADP + H^+$
Model	*Quasi-Steady-State Saturation Kinetic model*
Mathematical Equations	$\frac{dG6P}{dt} = v_{max} \cdot \frac{1}{\frac{k_M}{[G_{cell}]} + 1}$ $\frac{dG_{cell}}{dt} = -\frac{dG6P}{dt}$ $\frac{dATP}{dt} = -\frac{dG6P}{dt}$
v_{max} (mmol/kg min)	*1.0*
Regulation of k_M (mM)	
$k_{M,0}$	*0.1*
Inhibition Term	$[G6P]_N$-*0.9*
Scaling Factor (Inhibition)	*0.0040*

Pyruvate from G6P

The process of glycolysis in the adipose cell is the same as in the Metabolically-Active Tissue except that some of the G3P is used to synthesize TriG instead of pyruvate. Because of this divergence in the pathway at G3P, glycolysis in Adipose Tissue is split into two parts: synthesis of G3P from G6P, and synthesis of pyruvate from G3P. According to Newsholme and Leech (1983, p. 612), unlike in the Metabolically-Active Tissue, in which the rate of glycolysis is governed by 6PFK, in the Adipose Tissue submodel, the rate of glycolysis is governed by the rate of glucose uptake. We therefore use a maximal, substrate-limited model to describe G6P-to-G3P and G3P-to-Py processes in Adipose Tissue (see Table 30 and Table 31). The kinetic models for the two processes are from Stryer (1995, p. 491). For now we assume v_{max} is the same as for glucose phosphorylation (i.e., 1 mmol/min/kg).

Table 30 - Model Description: G3P from G6P (Adipose Tissue)

Kinetic Model	$G6P + ATP \xrightarrow{6PFK} 2G3P + ADP + H^+$
Model	*Maximal, Substrate-Limited Model*
Mathematical Equations	$\frac{dG3P}{dt} = \begin{cases} \frac{dG6P_{avail}}{dt} & for \quad \frac{dG6P_{avail}}{dt} \le v_{max} \\ v_{max} & for \quad \frac{dG6P_{avail}}{dt} > v_{max} \end{cases}$ $\frac{dG6P}{dt} = -\frac{dG3P}{dt}$ $\frac{dATP}{dt} = -\frac{1}{2} \cdot \frac{dG3P}{dt}$
v_{max} (mmol/kg min)	*1.0*

Table 31 - Model Description: Pyruvate from G3P (Adipose Tissue)

Kinetic Model	$G3P + 2ADP + NAD^+ + P_i \longrightarrow$ $Py + 2ATP + NADH + H^+ + H_2O$
Model	*Maximal, Substrate-Limited Model*
Mathematical Equations	$\frac{dPy}{dt} = \begin{cases} \frac{dG3P_{avail}}{dt} & for \quad \frac{dG3P_{avail}}{dt} \le v_{max} \\ v_{max} & for \quad \frac{dG3P_{avail}}{dt} > v_{max} \end{cases}$ $\frac{dG3P}{dt} = -\frac{dPy}{dt}$ $\frac{dATP}{dt} = -2 \cdot \frac{dPy}{dt}$ $\frac{dNADH}{dt} = \frac{dPy}{dt}$
v_{max} (mmol/kg min)	*1.0*

ACoA from Pyruvate

The metabolic pathway from pyruvate to ACoA is also the same as in the Metabolically-Active Tissue (see Stryer, 1995, p. 498 for the kinetic model). Pyruvate is transferred to the mitochondrion where it is converted to ACoA. It is likely that this process is controlled by insulin (Newsholme and Leech, 1983, p. 612).

However, given that glucose uptake (which is also controlled by insulin) is the rate-limiting step for glucose-to-TriG conversion, for simplification we assume a maximal, substrate-limited model. The model description is provided in Table 32, below.

Table 32 - Model Description: ACoA from Pyruvate (Adipose Tissue)

Kinetic Model	$CoA + Py + NAD^+ \longrightarrow ACOA + NADH + CO_2$
Model	*Maximal, Substrate-Limited Model*
Mathematical Equations	$\frac{dACoA}{dt} = \begin{cases} \frac{dPy_{avail}}{dt} & for \quad \frac{dPy_{avail}}{dt} \le v_{max} \\ v_{max} & for \quad \frac{dPy_{avail}}{dt} > v_{max} \end{cases}$ $\frac{dPy}{dt} = -\frac{dACoA}{dt}$ $\frac{dCoA}{dt} = -\frac{dACoA}{dt}$ $\frac{dNAD^+}{dt} = -\frac{dACoA}{dt}$

aCoA from ACoA

ACoA is formed in the mitochondria. ACoA must be transported back into the cytosol to participate in lipogenesis. There is no specific transport system for ACoA transport across the mitochondrial membrane. Two shuttles exist which could bring about net ACoA transport in adipose tissue, one using acetyl carnitine, and the other using citrate, with citrate being the most important. In the mitochondria, ACoA condenses with oxaloacetate to form citrate. Note that this is the first step in the citric acid cycle. In adipose tissue however, most (90%) of the citrate produced in the mitochondria is transported to the cytosol via the tricarboxylate carrier. In the cytosol, ACoA is re-formed from citrate in a reaction catalyzed by ATP citrate lipase. Again, because glucose uptake is the rate-limiting step, for simplification we assume a maximal, substrate-limited model.

The model description is provided in Table 33, below.

Table 33 - Model Description: aCoA from ACoA (Adipose Tissue)

Kinetic Model	$8ACoA + 7ATP + 14NADPH + 6H^+ \rightarrow C_{16}aCoA + 14NADP + 8CoA + 6H_2O + 7ADP + 7P_i$
Model	*Maximal, Substrate-Limited Model*
Mathematical Equations	$\frac{dC_{16}aCoA}{dt} = \begin{cases} \frac{dACoA_{avail}}{dt} & for \quad \frac{dACoA_{avail}}{dt} \le v_{max} \\ v_{max} & for \quad \frac{dACoA_{avail}}{dt} > v_{max} \end{cases}$ $\frac{dACoA}{dt} = -8\frac{dC_{16}aCoA}{dt}$ $\frac{dATP}{dt} = -7\frac{dC_{18}aCoA}{dt}$ $\frac{dNADPH}{dt} = -14\frac{dC_{18}aCoA}{dt}$ $\frac{dCoA}{dt} = -\frac{dACoA}{dt}$

TriG from aCoA

TriG is created by combining three aCoA with glycerol-3-phosphate (G3P) and water (see Stryer, 1995, p. 686). G3P can originate either from the phosphorylation of glycerol during lipogenolysis (see next subsection), or from the glycolytic pathway (Newsholme and Leech, 1983, p. 622). In the liver, the enzyme catalyzing the phosphorylation of glycerol is plentiful. This is not the case in adipose cells. Therefore, in the Adipose Tissue submodel, we consider that G3P comes only from the glycolytic pathway. This requires that glucose be simultaneously available within the cell. Thus, we assume a maximal, substrate-limited model in which the rate of lipogenesis is limited by the rate of G3P availability.

A description of the model is provided in Table 34, below.

Table 34 - Model Description: TriG from aCoA (Adipose Tissue)

Kinetic Model	$3aCoA + G3P + H_2O \longrightarrow TriG + 3CoA + P_i$
Model	*Maximal, Substrate-Limited Model*
Mathematical Equations	$\frac{dTriG}{dt} = \begin{cases} \frac{dG3P_{avail}}{dt} & for \quad \frac{dG3P_{avail}}{dt} \le v_{max} \\ v_{max} & for \quad \frac{dG3P_{avail}}{dt} > v_{max} \end{cases}$ $\frac{daCoA}{dt} = -3 \cdot \frac{dTriG}{dt}$ $\frac{dG3P}{dt} = -\frac{dTriG}{dt}$ $\frac{dCoA}{dt} = 3\frac{dTriG}{dt}$

TriG Degradation

The TriG stored in adipose tissue is an enormous source of metabolic fuel. TriG is broken down to FA and glycerol via hydrolysis (Newsholme and Leech, 1983, p. 262; Stryer, 1995, p. 605). The overall rate of the reaction is determined by TriG lipase (Newsholme and Leech, 1983, p. 262). According to Stryer (1995), this lipase is regulated by epinephrine, norepinephrine, glucagon, and adrenocorticotropic hormone. These hormones stimulate cAMP, which activates the lipase by phosphorylating it. Insulin inhibits lipolysis. Fatty acid mobilization from adipose tissue may also be under neural control working on local stores of norepinephrine, since denervation decreases the rate of mobilization, and sympathetic stimulation increases the rate of mobilization (Newsholme and Leech, 1983, p. 348). Because of the large store of TriG in the adipose cells, TriG degradation is effectively controlled by controlling the mass action rate coefficient, k. We assume that the resting rate of TriG degradation is sufficient to maintain FA_{blood} at 0.363 mM, given a resting FA utilization rate of 0.407 mmol/min by the Metabolically-Active Tissue (see previous section).

We assume that the rate of TriG degradation increases whenever epinephrine or glucagon are elevated, to attain a maximum level of 2.0 mmol/min of FA available for utilization, corresponding to approximately 25% of $VO_{2,max}$.($VO_{2,max}$ = 4.4 L/min). A description of the model is provided in Table 35, below.

Table 35 - Model Description: TriG Degradation (Adipose Tissue)

Kinetic Model	$TriG + 3H_2O \xrightarrow{k} Glycerol + 3FA + 3H^+$
Model	*Mass Action*
Mathematical Equations	$\frac{dTriG}{dt} = -k[TriG]$ $\frac{dFA}{dt} = -3\frac{dTriG}{dt}$ $\frac{dGlycerol}{dt} = -\frac{dTriG}{dt}$
Regulation of k (mmol/min/mM) k_0 Activation Factor Scaling Factor	 *0.00013553* *(Epinephrine$_N$ - 1) + (Glucagon$_N$ – 1)* *15000*

Testing

Testing has not been completed for this subsystem model.

Discussion

There is not nearly as much quantitative information on adipose tissue cells as on metabolically-active tissue. On the other hand, the adipose tissue cells represent a simpler problem. TriG in adipose cells represents a huge store of metabolic fuel, so that the absolute time it takes for ingested fats to be stored in the adipose cells is relatively unimportant. What is important about the storage process is that glucose not be taken up by the adipose tissue cells and that TriG not be produced in large amounts during exercise or when glucose is in short supply. This may lead to simplification of the adipose tissue cells in future versions of DYNUMO. The rate of degradation of TriG in Adipose Tissue determines, for the most part, the rate of fatty acid metabolism in Metabolically-Active Tissue, which largely determines the rate of carbohydrate utilization. Therefore, the rate of TriG degradation must be known with a relatively high degree of certainty.

LIVER TISSUE

One of the primary functions of the liver is to convert, store, and release metabolic fuels for use by other tissues. The metabolic pathways considered in this section are shown below, in Figure 18:

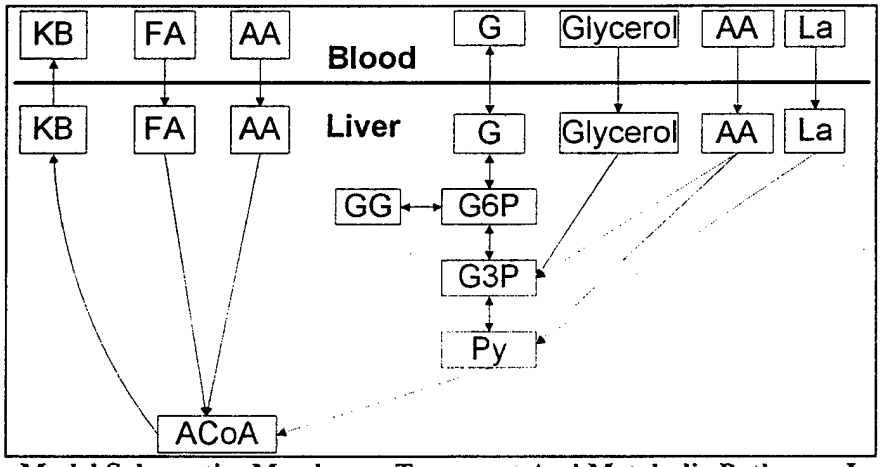

Figure 18 - Model Schematic: Membrane Transport And Metabolic Pathways In The Liver Tissue Submodel

Although the liver can use metabolic fuels to generate ATP for its own use, that function is less significant than that of storing and converting metabolic fuels for use by other tissues and will not be considered here. In this simplified model, the liver takes up glucose, stores it as glycogen, converts the glycogen back to glucose, and releases the glucose into the blood for use by other tissues. The liver also takes up and converts lactate, pyruvate, glycerol, and certain amino acids into glucose by the process of gluconeogenesis (which aids in maintaining blood glucose levels). Lipid metabolism, including generation of VLDL, TriG and ketone bodies and storage of TriG are ignored for the present time.

At this time, the liver model has not been implemented in DYNUMO. Coding has been completed assuming either quasi-steady-state saturation kinetic models or mass action models for all pathways. Parameter values and regulation mechanisms have not yet been identified.

Initial Conditions

Compartment Volume and Mass

Liver weight equals approximately 2.3 g/100g body weight (Derelanko, 1995). This amounts to 1.61 kg for a 70 kg man. Using a tissue density of 1.1 g/ml, the resulting compartment volume is 1.46 liters.

Concentrations

Identification or derivation of initial values for substances considered in the liver tissue model is incomplete.

Values obtained thus far are provided below, in Table 36, below.

Table 36 - Initial Concentrations-Liver Tissue Model

Symbol	Description	Initial Value (mM)	Reference
G_{cell}	Cellular Glucose	5	derived
G6P	Glucose-6-Phosphate		
G3P	Glyceraldehyde 3 Phosphate		
Py	Pyruvate		
CoA	Coenzyme A		
ACoA	Acetyl Coenzyme A		
aCoA	Acyl Coenzyme A		
KB	Ketone Body		
AA	Amino Acid		
Glycerol	Glycerol		
La	Lactate		
GG	Glucose Stored As Glycogen	330	derived
FA_{cell}	Cellular Fatty Acid		

The value for $[G_{cell}]$ was derived by assuming the intracellular glucose concentration is near equilibrium with glucose in the blood. The value for glycogen concentration (330 mM) was derived from a value of 300 mmol/kg provided in Hultman (1978), assuming a tissue density of 1.1 g/ml. The remaining concentrations have yet to be identified.

Resting Rates of Substrate Uptake and Product Release

Resting rates of substrate uptake and product release have not yet been identified.

Glucose Metabolism

Glucose metabolism in the liver includes processes to take up glucose, to convert it to glycogen for storage, and to release glucose into the blood. ATP synthesis from glucose is considered in the Metabolically-Active Tissue model and will not be considered here.

Glucose Uptake and Release

The GLUT1 and GLUT3 glucose transporters (k_M = 1.0 mM) are present in nearly all body tissues, including liver (Stryer, 1995, p. 505). Liver also has GLUT2 transporters (k_M=15-20 mM) that are present only in liver and pancreatic tissue (Stryer, 1995, p. 505). The overall affinity for glucose is relatively low, so that the rate of transport is proportional to G_{blood} until G_{blood} exceeds approximately 20 mM. The high k_M value also results in preferential uptake of glucose by muscle and brain when blood glucose is low. The effect of insulin regulation on glucose uptake is small compared to the effect of changes in glucose concentration. Therefore, we assume a simple, unregulated model. Richter et al. (1986) provides evidence that hepatic glucose uptake may be partially controlled by epinephrine. This observation has not yet been incorporated into the model. We currently do not have information for v_{max} in the liver. We will assume a value of approximately 1.5 mmol/kg/min provided in Newsholme and Leech (1983, p. 181). We use a value for k_M of 15 mM, which is the lower value given for the GLUT2 transporter (Stryer, 1995, p. 505).

The details of the model are provided in Table 37.

Table 37 - Model Description: Glucose Uptake and Release (Liver)

Kinetic Equation	$G_{blood} \xleftarrow{carrier} G_{cell}$
Model	*Quasi-Steady-State Saturation Kinetic model*
Mathematical Equations	$\frac{dG_{cell}}{dt} = \frac{v_{max}}{\frac{k_M}{[G_{blood}]}+1} - \frac{v_{max}}{\frac{k_M}{[G_{cell}]}+1}$ $\frac{dG_{blood}}{dt} = -\frac{dG_{cell}}{dt}$
v_{max} (mmol/kg min)	*1.5*
k_M (mM)	*15*

Glucose Phosphorylation and Reverse

In Metabolically-Active Tissue, glucose phosphorylation is catalyzed by hexokinase which has a low k_M for glucose (approximately 0.1 mM), is usually saturated with substrate, and is inhibited by its product, G6P. In contrast, in the liver, glucose phosphorylation is catalyzed by glucokinase, which has a high k_M for glucose (approximately 10 mM according to Stryer, 1995, p. 495), is typically not saturated with substrate, and is not inhibited by G6P. The high k_M ensures that the activity of the enzyme varies in approximate proportion to the concentration of hepatic glucose, which is itself in near equilibrium with glucose in the blood. Therefore, the higher the glucose concentration in the hepatic portal vein, the greater the rate of glucose phosphorylation (Newsholme and Leech, 1983, p. 460-461). The hepatic portal vein, which provides up to 70% of the blood reaching the liver, drains most of the absorptive area of the intestine so that after a carbohydrate-containing meal, the largest changes in blood glucose will appear in this vein.

In addition to differences between hexokinase and glucokinase, glucose phosphorylation in liver differs significantly from glucose phosphorylation in other tissues in that the process is reversible. In the liver, both the forward reaction, catalyzed by glucokinase (GKase), and the reverse, catalyzed by glucose-6-phosphatase (G6Pase), are simultaneously active; the relative reaction rates determine the net response. Both also have approximately the same affinity for glucose, with k_M values of approximately 10 mM (Stryer, 1995, p. 495; Newsholme and Leech, 1983, p. 433). When both reaction rates are high, the sensitivity to control is greatly enhanced. This may explain how the liver can change both the rate and the direction of glucose metabolism in response to small changes in blood glucose concentration (Newsholme and Leech, 1983, p.461). Note however, that conversion of G_{cell} to G6P requires ATP, which is not replenished on conversion of G6P to G_{cell}. Therefore, this particular regulation scheme is accomplished at the expense of ATP consumption. The kinetic models for the forward and reverse reactions come from Stryer (1995), pp. 491 and 571, respectively. We have not yet identified values for v_{max}.

The details of the model are provided in Table 38, below.

Table 38 - Model Description: Glucose Phosphorylation and Reverse (Liver)

Kinetic Equations	$Gcell + ATP \xrightarrow{GKase} G6P + ADP + H^+$ $G6P + H_2O \xrightarrow{G6Pase} Gcell + P_i$
Model	*Quasi-Steady-State Saturation Kinetic model*
Mathematical Equations	$\frac{dG6P}{dt} = \left(\frac{v_{max}}{\frac{k_{M,Gcell}}{[G_{cell}]} + 1} \right)_{Gkase} - \left(\frac{v_{max}}{\frac{k_{M,G6P}}{[G6P]} + 1} \right)_{G6Pase}$ $\frac{dG_{cell}}{dt} = -\frac{dG6P}{dt}$ $\frac{dATP}{dt} = -\left(\frac{v_{max}}{\frac{k_{M,Gcell}}{[G_{cell}]} + 1} \right)_{Gkase}$
Parameter Values $v_{max,GKase}$ (mmol/min) $v_{max,G6Pase}$ (mmol/min) $k_{M,GKase}$ (mM) $k_{M,G6Pase}$ (mM)	 *10.0* *10.0*

Glycogen Synthesis and Degradation

The processes of glycogen synthesis and degradation are the same as in the Metabolically-Active Tissue. Whereas the purpose of glycogen storage in the Metabolically-Active Tissue is to provide a glucose reserve for use during high-energy demand, the purpose of hepatic glycogen storage is to provide a glucose reserve to maintain the blood glucose concentration. It is assumed that glucagon increases the rate of glycogen degradation (Newsholme and Leech, 1983, p. 458), while insulin reduces this effect (Newsholme and Leech, 1983, p. 459). Epinephrine also increases glycogen degradation, but through a different mechanism than glucagon (Newsholme and Leech, 1983, p. 459). An increase in intracellular glucose decreases the activity of the phosphorylase and increases the activity of glycogen synthase, promoting glycogen synthesis (Newsholme and Leech, 1983, p. 461-463).

The kinetic model for glycogen synthesis was found in Stryer (1995, p. 588). The details of the model are provided in Table 39, below.

Table 39 - Model Description: Glycogen Synthesis (Liver)

Kinetic Model	$G6P + G6P + GG_n + H_2O \xrightarrow{GG-synthase} GG_{n+1} + ADP + 2P_i$
Model	*Quasi-Steady-State Saturation Kinetic model*
Mathematical Equations	$\frac{dG6P}{dt} = -v_{max} \cdot \frac{1}{\frac{k_M}{[G6P]}+1}$ $\frac{dGlycogen}{dt} = -\frac{dG6P}{dt}$

The kinetic model for glycogen degradation was found in Stryer (1995, p. 583-585). The details of the model are provided in Table 40, below.

Table 40 - Model Description: Glycogen Degradation (Liver)

Kinetic Model	$GG_n + P_i \longrightarrow GG_{n-1} + G6P$
Model	*Quasi-Steady-State Saturation Kinetic model*
Mathematical Equations	$\frac{dG6P}{dt} = -\frac{v_{max}}{\frac{k_M}{[GG]}+1}$ $\frac{dGG}{dt} = -\frac{dG6P}{dt}$

Gluconeogenesis

As stated previously, an important metabolic function of the liver is to store metabolic fuels and to convert non-carbohydrate fuels into glucose for use by other tissues. Glucose, which is critical for brain tissue and for anaerobic metabolism, can be generated, through the process of gluconeogenesis, from several other fuels including pyruvate, lactate, glycerol, and certain amino acids. The glucose that is produced can then be released into the blood. The gluconeogenic pathway (Figure 19) converts pyruvate into glucose. Non-carbohydrate precursors enter the pathway at pyruvate, oxaloacetate or G3P.

Gluconeogenesis can be considered a partial reversal of glycolysis. Most glycolytic reactions are near-equilibrium and can be readily reversed by small changes in substrate or product concentration. However, two of the glycolytic reactions are non-equilibrium; reversal of these reactions would require large changes in substrate or product concentration that might not be physiologically feasible. Instead, reversal of these reactions for gluconeogenesis is accomplished using different mechanisms altogether.

Of the individual reactions making up the gluconeogenic pathway, there is no apparent rate-determining step. Instead, the reaction rate is determined largely by the availability of precursors (Newsholme and Leech, 1983, p. 447). Availability of precursors, in turn, is determined by the rates of lactate and amino acid release from muscle, and glycerol release from adipose tissue. Adequate levels of ATP are required for the gluconeogenic process to continue.

Aside from availability of substrate, gluconeogenesis is regulated indirectly through regulation of the glycolytic pathway. Factors that increase the rate of glycolysis slow down the rate of gluconeogenesis, and factors that inhibit glycolysis speed up the rate of gluconeogenesis. Therefore, insulin generally decreases and glucagon generally increases the rate of gluconeogenesis. Glucocorticoids appear to have no effect on gluconeogenesis on their own, but enhance the effect of changes brought about by other hormones (Newsholme and Leech, 1983, p. 452). High ATP/ADP ratios, ACoA/CoA ratios, and citrate concentrations, which regulate glycolysis, may activate gluconeogenesis. Because we are not considering ATP generation in liver, these factors are not considered here.

We first consider the conversion of pyruvate to G6P, then the reactions specific to each of the non-carbohydrate precursors.

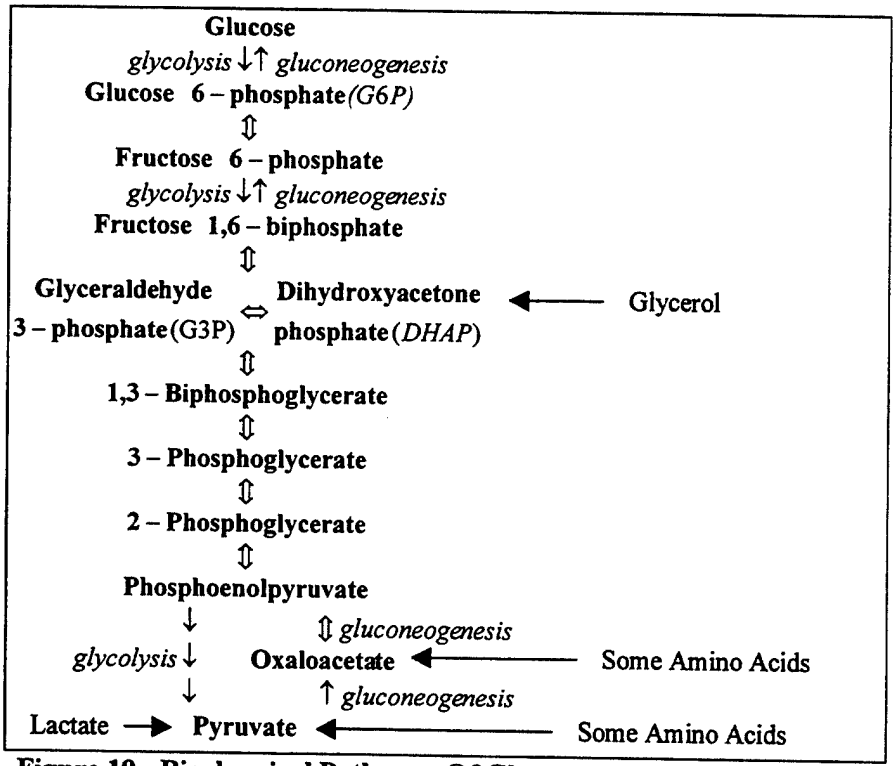

Figure 19 - Biochemical Pathways Of Gluconeogenisis And Glicolysis

Gluconeogenesis from Pyruvate

Gluconeogenesis from pyruvate is considered to occur in two separate steps to account for the entry of glycerol into the pathway at the level of G3P: generation of G3P from

pyruvate and generation of G6P from G3P. The kinetic models for these two processes come from Stryer (1995), pp. 491 and 571, respectively. We currently do not have any information on v_{max} or k_M values. The details of these models are provided in Table 41 and Table 42.

Table 41 - Model Description: G3P from Pyruvate (Liver)

Kinetic Model	$Py + 3ATP + 2H_2O + NADH \longrightarrow G3P + 3ADP + NAD^+ + 2P_i$
Model	*Quasi-Steady-State Saturation Kinetic model*
Mathematical Equations	$\frac{dG3P}{dt} = \frac{v_{max}}{\frac{k_M}{[Py]} + 1}$ $\frac{dPy}{dt} = -\frac{dG3P}{dt}$ $\frac{dATP}{dt} = -3\frac{dG3P}{dt}$

Table 42 - Model Description: G6P from G3P (Liver)

Kinetic Model	$2G3P + H_2O \longrightarrow G6P + P_i$
Model	*Quasi-Steady-State Saturation Kinetic model*
Mathematical Equations	$\frac{dG6P}{dt} = \frac{v_{max}}{\frac{k_M}{[G6P]} + 1}$

Gluconeogenesis from Lactate

Approximately 120 g of lactate are produced on a daily basis. The amount of lactate produced by muscle increases dramatically with activity level (Newsholme and Leech, 1983, p. 448). The blood concentration of lactate is approximately 1.0 mM, which represents the balance among production in muscle, oxidation in heart and red muscle (Newsholme and Leech, 1983, p. 448) and uptake for gluconeogenesis in liver. This subsection describes only the uptake of lactate from the blood and the conversion of lactate to pyruvate in the liver; conversion of this pyruvate to G6P is described in the previous subsection.

Lactate Uptake

We have not obtained specific information regarding lactate uptake in the liver. For now, we assume a simple diffusion model as shown in Table 43.

Table 43 - Model Description: Lactate Uptake (Liver)

Kinetic Model	$LA_{blood} \overset{k}{\longleftrightarrow} LA_{cell}$
Model	*Mass Action*
Mathematical Equations	$\frac{dLA_{cell}}{dt} = k([LA_{blood}] - [LA_{cell}])$

Pyruvate from Lactate

The model for obtaining pyruvate from lactate is shown below, in Table 44. Note that the reaction is reversible. The rate-limiting factor for gluconeogenesis is the appearance of substrate. Therefore, we use a maximal, substrate-limited model to describe this process. The kinetic model was found in Stryer (1995, p. 497).

Table 44 - Model Description: Pyruvate from Lactate (Liver)

Kinetic Model	$LA + NAD^+ \longleftrightarrow Py + NADH + H^+$
Model	*Maximal, Substrate-Limited*
Mathematical Equations	$\frac{dPy}{dt} = \begin{cases} \frac{dLa_{avail}}{dt} & for \quad \frac{dLa_{avail}}{dt} \le v_{max} \\ v_{max} & for \quad \frac{dLa_{avail}}{dt} > v_{max} \end{cases}$ $dLa = -\frac{dPy}{dt}$ $dNADH = \frac{dPy}{dt}$

Gluconeogenesis from Glycerol

Glycerol is produced during the breakdown of triacylglycerol in the blood and in adipose tissue. In a fasting, resting man, 19 g of glycerol is released per day, and almost all of this is converted to glucose by the liver. The rate of glycerol release is increased during exercise or stress (Newsholme and Leech, 1983, p. 449). The process of gluconeogenesis from glycerol involves the uptake of glycerol from the blood and conversion of glycerol to G3P. Conversion of this G3P to G6P is described in the subsection 'Gluconeogenesis from Pyruvate'.

Glycerol Uptake

The model for glycerol uptake is shown in Table 45. It is unclear whether glycerol enters the cell using a specific transport system or by simple diffusion. For now, we assume simple diffusion.

Table 45 - Model Description: Glycerol Uptake (Liver)

Kinetic Model	$Glycerol_{blood} \overset{k}{\longleftrightarrow} Glycerol_{cell}$
Model	*Mass Action*
Mathematical Equations	$\frac{dGlycerol_{cell}}{dt} = k([Glycerol_{blood}] - [Glycerol_{cell}])$

G3P From Glycerol

Once inside the cell, glycerol is phosphorylated to form glycerol-3-phosphate (G3P). The rate-limiting factor for gluconeogenesis from glycerol is the appearance of substrate. Therefore, we use a maximal, substrate-limited model to describe this pathway. The

kinetic model was obtained from Stryer (1995, pp. 606 and 491). The details of the model are provided in Table 46, below.

Table 46 - Model Description: G3P from Glycerol (Liver)

Kinetic Equations	$Glycerol + ATP \longrightarrow G3P + ADP + H^+$
Model	*Maximal, Substrate-Limited*
Mathematical Equations	$\frac{dG3P}{dt} = \begin{cases} \frac{dGlycerol_{avail}}{dt} & for \quad \frac{dGlycerol_{avail}}{dt} \le v_{max} \\ v_{max} & for \quad \frac{dGlycerol_{avail}}{dt} > v_{max} \end{cases}$ $dGlycerol = -\frac{dG3P}{dt}$ $dATP = -\frac{dG3P}{dt}$

Gluconeogenesis from Amino Acids

Glucogenic amino acids can be catabolized to pyruvate or oxaloacetate, either of which can be converted to glucose in the liver. Alanine, released from muscle and small intestine, is quantitatively the most important amino acid precursor for gluconeogenesis in the liver (Newsholme and Leech, 1983, p. 450). The process of gluconeogenesis from amino acids includes the uptake of amino acid, the conversion of the amino acid to an intermediate of the 'Gluconeogenesis from Pyruvate' process (which may actually involve several more steps), and gluconeogenesis from this intermediate step.

Amino Acid Uptake

Amino acid uptake requires an active carrier system. At least seven such carriers are known to exist (Newsholme and Leech, 1983, p.398). To simplify, we assume that the system can be represented by the alanine carrier system. The model for this system is described in Table 47, below.

Table 47 - Model Description: Amino Acid Uptake (Liver)

Kinetic Model	$AA_{blood} + ATP \xrightarrow{k} AA_{cell} + ADP$
Model	*Mass Action*
Mathematical Equations	$\frac{dAA_{cell}}{dt} = k([AA_{blood}][ATP])$ $\frac{dAA_{blood}}{dt} = -\frac{dAA_{cell}}{dt}$ $\frac{dATP}{dt} = -\frac{dAA_{cell}}{dt}$

Pyruvate From Amino Acid

For simplicity, we will assume that all gluconeogenic amino acids enter the gluconeogenic pathway at pyruvate. The rate-determining step for gluconeogenesis from

amino acids is the availability of amino acid. Thus, a maximal, substrate-limited model is used to describe this process. The kinetic model (for conversion of alanine to pyruvate) was obtained from Stryer (1995, p. 630). The details of the model are provided in Table 48, below.

Table 48 - Model Description: Pyruvate from Amino Acid (Liver)

Kinetic Model	$AA + H_2O + NAD^+ \longrightarrow Py + NADH + NH_4^+ + H^+$
Model	*Maximal, Substrate-Limited*
Mathematical Equations	$\frac{dPy}{dt} = \begin{cases} \frac{dAA_{avail}}{dt} & for \quad \frac{dAA_{avail}}{dt} \le v_{max} \\ v_{max} & for \quad \frac{dAA_{avail}}{dt} > v_{max} \end{cases}$ $dAA = -\frac{dPy}{dt}$ $dNADH = \frac{dPy}{dt}$

Testing

Testing has not been completed for this subsystem model.

Discussion

Parameter value estimation and submodel testing have not been completed for this submodel. The processes of ketogenesis and lipid metabolism have not been included. These processes are important during prolonged caloric, particularly carbohydrate deficits and will be implemented in future versions of DYNUMO.

REGULATORY SYSTEM

Metabolic regulation is achieved by altering the rates of key metabolic reactions. Much of this regulation is achieved by local factors (e.g., substrate and product concentrations, as well as the presence of other molecules in the immediate area), which has been described in previous sections. Regulation by centrally produced factors, such as epinephrine, norepinephrine, insulin, glucagon, and glucocorticoid hormones also occurs. The Regulatory System submodel currently incorporates processes for insulin, glucagon, and epinephrine production, which are described below. The effects of insulin, glucagon, and epinephrine on metabolism are covered in preceding sections.

Initial Conditions

Initial conditions for the Regulatory System were found in Newsholme and Leech (1983, p. 372) and are provided in Table 49. Concentrations are given per volume of blood (V_{blood}). Initial values assume a healthy, rested, well-fed individual.

Table 49 - Initial Conditions - Regulatory System

Symbol	*Description*	*Initial Value*	*Units*
Insulin	Insulin	14	μU/ml
Glucagon	Glucagon	80	pg/ml
Epinephrine	Epinephrine	0.1	ng/ml
$Insulin_N$	Normalized Insulin	1.0	na
$Glucagon_N$	Normalized Glucagon	1.0	na
$Epinephrine_N$	Normalized Epinephrine	1.0	na

Insulin

In general, insulin is produced during times of carbohydrate excess and works to enhance storage of glucose as glycogen or triacylglycerol and to inhibit gluconeogenesis. When the body is at rest, insulin is secreted by the alpha cells of the islets of Langerhans (Newsholme and Leech, 1983, p. 572) in response to increased blood glucose levels. The simplest representation of the insulin response to changes in blood glucose is a proportional control system:

$$Insulin_N = \left(G_{blood,N} - 1\right) \cdot \eta + 1$$

Data from Thomas and co-workers (1991) were used to develop the parameter values for the relationship between the normalized insulin value ($Insulin_N$) and the normalized blood glucose concentration ($G_{blood,N}$). In this study, subjects consumed lentils, potatoes, or glucose (1 gram of available CHO per kg of body mass) plus water, making the total volume of the meal 400 ml. The blood glucose and insulin responses to each meal were measured at 15-minute intervals for one hour. From this data, the proportionality coefficient (η) was found to be approximately 3.4. Because insulin release is inhibited

when exercise exceeds 50% of $VO2_{max}$ (Galbo, 1983; Wahren et al., 1971), η is set to zero when the activity level exceeds 50% of $\dot{V}O_{2,max.}$

In hormonal control, there is typically a time delay between the time that the change in the regulated variable is detected and the time when the hormone is delivered to the effector area. In the case of insulin, however, the delay appears to be very slight or non-existent. There is some evidence that insulin release is stimulated by changes in intestinal carbohydrate level as well as by changes in blood glucose level, meaning that insulin responds in an anticipatory fashion to increases in blood glucose that follow a meal. For this reason, no time delay was added to the model.

Glucagon

Both glucagon and insulin are secreted by the cells of the islets of Langerhans, the former from the alpha cells and the latter from the beta cells. Glucagon is generally produced during times of carbohydrate depletion and generally has opposite affects of insulin; glucagon favors the release of glucose into the blood, glycogen degradation, and gluconeogenesis. We do not currently have data for relating glucagon to G_{blood}. Using a model similar to the one used for insulin yields:

$$Glucagon_N = (1 - [G_{blood}]_N) \cdot \eta_G + 1$$

where $Glucagon_N$ is the normalized value for glucagon, η_G is the proportionality coefficient, and $[G_{blood}]_N$ is the normalized blood glucose concentration. Unlike insulin, glucagon is not inhibited during exercise, typically increasing toward the end of prolonged exercise when blood glucose concentration is low (Galbo, 1983). Blood glucose is typically 4.0 mM in a fasting man, which is one mM lower than the normal or set-point value of 5.0 mM. This indicates a system that is perhaps more sensitive to a drop in blood glucose than an increase.

Epinephrine

Epinephrine is released under a variety of conditions including exercise and stress. An exponential relationship between the normalized epinephrine value and exercise intensity is assumed.

$$Epinephrine_N = e^{0.373(\%VO2_{max} - \%VO2_{max,rest})}$$

The exponential coefficient of 0.0373 was obtained assuming that $Epinephrine_N$ is 1.0 at rest, is 1.5 at 25% of VO2max (Martin, 1996), is 3-6 at 65% of VO2max, and is 17-19 at 85% of VO2max (Romijn et al., 1993).

Note that this relationship does not account for changes in epinephrine release that occur over time, during constant work exercise protocols. It is known that during short-term

exercise, plasma epinephrine does not increase above resting levels for activity levels below approximately 60% of VO2max (Richter et al., 1986). However, during prolonged exercise, epinephrine is observed at activity levels lower than 60% of $VO2_{max}$, later in the exercise period. What causes the epinephrine release later in exercise is not known. The model above accounts for epinephrine release at lower activity levels, although the time course of epinephrine release may not be accurate. The user may override the computed epinephrine value to account for other stresses.

CONCLUSIONS AND RECOMMENDATIONS

During the period February, 2000 through December, 2000, models of the major biochemical pathways for each subsystem were developed. Preliminary parameter value estimation and limited functional testing were conducted for the Digestive System and the Metabolically-Active Tissue. Parameter value estimation for the Central Blood Compartment, Adipose Tissue and Liver Tissue subsystems was not completed.

Detailed discussions of model assumptions are offered in previous sections. A review of some of the more important assumptions and limitations is provided in Table 50, below.

Table 50 - Review of model assumptions and known limitations

Model or Submodel	*Assumptions or Limitations*
General	• Biochemical pathways represented by single representative reactions • Briggs/Haldane model used for most reactions • Maximal, substrate-limited model used for "fast" reactions • Pipeline model used for "slow" reactions • Enzyme control achieved by modifying reaction coefficients
Central Blood Compartment	• Parameter estimation not yet complete
Digestive System	• Food consumed as bolus • Gastric emptying described by exponential model (Hunt and Stubbs, 1975) • Limited data set for gastric emptying – predominantly single-ingestion experiments, predominantly glucose solutions • Digestion/Absorption dynamics described by a pipeline model • Very limited data set for digestion/absorption – exclusively glucose solutions • Protein digestion and absorption not yet included • Carbohydrates and lipids are released into the blood as glucose and triacylglycerol; disaccharide, fructose or other lipid (e.g., cholesterol, fatty acid, VLDL, and HLDL) products not considered • Effects of dietary fiber, hydration, and electrolytes not yet included • All ingested nutrients eventually absorbed • Limits on rates of absorption (Duchman et al., 1997) not yet implemented. • Effects of exercise or physical activity not included.
Metabolically-Active Tissue	• Triacylglycerol storage and use in muscle not yet considered • Represented by skeletal muscle characteristics • Enzymes controlled by Ca^{2+} and epinephrine are modeled by relating V_{max} to MetRate; end product inhibition and other local regulatory mechanisms fine tune the pathway • Active and inactive muscle (along with other cell types) are represented by a single compartment • Phosphocreatine not yet considered • Use of carbohydrate to replenish citric acid cycle intermediates (i.e., anaplerotic reactions) not yet considered • Changes in substrate concentration based on organ volume, not on diffusion space

Table 50 Cont'd

Adipose Tissue	• Energy consumption ignored • Parameter value estimation not yet conducted
Liver Tissue	• Energy consumption ignored. • Parameter value estimation not yet conducted
Regulatory System	• Three factors considered: insulin, glucagon, epinephrine • Insulin and glucagon are linearly related to blood glucose • Epinephrine related to relative exercise intensity

Most of the attention during the period December, 2000 - February, 2000, was devoted to the Digestive System and Metabolically-Active Tissue subsystems. In the future, it will be necessary to complete parameter estimation and functional testing of the remaining subsystem models. Also, to more accurately model the interaction between carbohydrate and fatty acid metabolism, anaplerotic reactions should be included in the Metabolically-Active Tissue submodel. It will also be necessary to perform formal testing of both the complete model and individual submodels.

The focus of model development has been on carbohydrate metabolism and scenarios of up to a few hours duration. The military operational environment often includes scenarios of extended duration (several days to a few weeks) during which time maintaining caloric balance is often not possible. To accurately simulate these scenarios, it will be necessary to accurately model the recovery period following physical activity and the processes that predominate during carbohydrate depletion, including gluconeogenesis, and amino acid and ketone body metabolism.

A few other modifications and additions may be necessary to expand the capabilities of DYNUMO. To more accurately simulate muscle glycogen depletion for a wide range of physical activities, it will probably be necessary to separate the Metabolically-Active Tissue compartment into active and inactive skeletal muscle, brain, and "other" compartments. To model performance of nonsteady-state or sequential tasks, it would be necessary to divide the muscle compartment into several compartments and to better model high intensity exercise (including phosphocreatine metabolism). To account for the effects of ergogenic aids on performance, it will be necessary to include phosphocreatine metabolism and to account for the effects of caffeine. To model the combined effects of multiple stressors, it will be necessary to develop a more detailed model of epinephrine release and its effects on metabolism.

This document reports research undertaken at the U.S. Army Soldier and Biological Chemical Command, Soldier Systems Center, and has been assigned No. NATICK/TR-03/006 in a series of reports approved for publication.

REFERENCES

Ahlborg, B.; Bergstrom, J.; Ekelund, L.G. Muscle glycogen and muscle electrolytes during prolonged physical exercise. Acta Physiol Scand 70:129-142, 1967.

Ahlborg, G.; Felig, P.; Hagenfeldt, L.; Hendler, R.; Wahren, J. Substrate turnover during prolonged exercise in man. Splanchnic and leg metabolism of glucose, free fatty acids, and amino acids. J Clin Invest 53:1080-1090, 1974.

Barker, G.R.; Cochrane, G.M.; Corbett, G.A.; Dufton, J.F.; Hunt, J.N.; Roberts, S.K. Glucose, glycine, and diglycine in test meals as stimuli to duodenal osmoreceptor slowing gastric emptying. J Physiol 283:341-346, 1978.

Barker, G.R.; Cochrane, G.M.; Corbett, G.A.; Hunt, J.N.; Roberts, S.K. Actions of glucose and potassium chloride on osmoreceptors slowing gastric emptying. J Physiol 237:183-186, 1974.

Benton, D.; Owens, D.S.; Parker, P.Y. Blood glucose influences memory and attention in young adults. Neuropsychologia 32(5):595-607, 1994.

Berger, M.; Hagg, S.; Ruderman, N.B. Glucose metabolism in perfused skeletal muscle. Interaction of insulin and exercise on glucose uptake. Biochem J 146: 231-238, 1975.

Bergstrom, J.; Hultman, E.A. Study of the glycogen metabolism during exercise in man. Scand J Clin Lab Invest 19:218-228, 1967.

Bonen, A.; Ness, G.W.; Belcastro, A.N.; Kirby, R.L. Mild exercise impedes glycogen repletion in muscle. J Appl Physiol 58:1622-1629, 1985.

Brener, W.; Hendrix, T.R.; McHugh, P.R. Regulation of gastric emptying of glucose. Gastroenterology 85:76-82, 1983.

Briggs, G.E.; Haldane, J.B.S. A note on the kinetics of enzyme action. Biochem J 19:338-339, 1925.

Brown, M.S.; Goldstein, J.L. Familial hypercholesterolemia: model for genetic receptor disease. Harvey Lect 73:163-201, 1979.

Brown, M.S.; Kovanen, P.T.; Goldstein, J.L. Regulation of plasma cholesterol by lipoprotein receptors. Science 212: 628-635, 1981.

Burke, E.R. Optimal Muscle Recovery. New York: Avery Publishing Group, 1999, p. 21.

Chatham, J.C.; Phil, D. Where Have All the Carbons Gone? Modeling TCA Cycle Fluxes - the Good, the Bad and the Unknown. http://www2.utsouthwestern.edu/rogersmr/John%20C.%20Chatham%201998.htm, University of Texas Southwestern Medical Center at Dallas, 2001

Conlee, R.K.; Hickson, R.C.; Winder, W.W.; Hagberg, J.M.; Holloszy, J.O. Regulation of glycogen resynthesis in muscles of rats following exercise. Am J Physiol (Reg Int Comp Physiol) 235: R145-R150, 1978.

Consolazio, C.F., R.E. Johnson, and L.J. Pecora. Physiological Measurements of Metabolic Functions in Man. New York: McGraw-Hill, 1963, p. 315.

Costil, D.L. Gastric emptying of fluids during exercise. In: Perspectives in Exercise Science and and Sports Medicine. Volume 3: Fluid Homeostasis During Exercise, C.V. Gisolfi and D.R. Lamb, eds. Indianapolis, IN: Benchmark Press Inc., 1990, pp. 97-121.

Costill, D.L.; Saltin, B. Factors limiting gastric emptying during rest and exercise. J Appl Physiol 37:679-683, 1974.

Cox, D.J.; Gonder-Frederick, L.A.; Schroeder, D.B.; Cryer, P.E.; Clarke, W.L. Disruptive effects of acute hypoglycemia on speed of cognitive and motor performance. Diabetes Care 16(10):1391-1393, 1993.

Coyle, E.F.; Costill, D.L.; Fink, W.J.; Hoopes, D.G. Gastric emptying rates for selected athletic drinks. Res Q 49:119-124, 1978.

Crapo, P.A.; Reaven, G.; Olefsky, J. Plasma glucose and insulin responses to orally administered simple and complex carbohydrates. Diabetes 25:741-747, 1976.

Derelanko, M.J. Risk Management. In: CRC Handbook of Toxicology, M.J. Derelanko and M.A. Hollinger, eds. 1995, p. 645.

Duchman, S.M.; Ryan, A.J.; Schedl, H.P.; Summers, R.W.; Bleiler, T.L.; Gisolfi, C.V. Upper limit for intestinal absorption of a dilute glucose solution in men at rest. Med Sci Sports Exerc 29(4):482-488, 1997.

Elias, E.; Gibson, G.J.; Greenwood, L.F.; Hunt, J.N.; Tripp, J.H. The slowing of gastric emptying by monosaccharides and disaccharides in test meals. J Physiol 194:317-326, 1968.

Felig, P.; Wahren, J. Fuel homeostasis in exercise. New Engl J Med 293:1078-1084, 1975.

Fordtran, F.S. Simulation of active and passive sodium absorption by sugars in the human jejunum. J Clin Invest 55:728-737, 1975.

Fordtran, J.S.; Ingelfinger, F.J Absorption of water electrolytes and sugars from the human gut. In: Handbook of Physiology – Alimentary Canal IV. Washington, D.C.: American Physiological Society, 1968, pp. 1457-1489.

Foster, C.; Costill, D.L.; Fink, W.J. Gastric emptying characteristics of glucose and glucose polymer solutions. Res Q 51:299-305, 1980.

Galbo, H.; Holst, J.J.; Christensen, N.J. Glucagon and plasma catecholamine responses to graded and prolonged exercise in man. J Appl Physiol 38:70-76, 1975.

George, J.D. New clinical method for measuring the rate of gastric emptying: the double sampling test meal. Gut 9:237-242, 1968.

Gisolfi, C.V.; Summers, R.D.; Schedl, H.P.; Bleiler, T.L. Effect of sodium concentration in a carbohydrate-electrolyte solution on intestinal absorption. Med Sci Sports Exerc 27(10):1414-1420, 1995.

Griffith, G.H.; Owen, G.M.; Campbell, H.; Shields, R. Gastric emptying in health and gastroduodenal disease. Gastroenterology 54:1-7, 1968.

Guyton, A.C. Basic Human Physiology: Normal Function and Mechanisms of Disease, 2nd Edition. Philadelphia: WB Saunders Co., 1977.

Harvey, R.F.; Mackie, D.B.; Brown, N.J.; Keeling, D.H.; Davies, W.T. Measurement of gastric emptying time with a gamma camera. Lancet 1(7636):16-8, 1970.

Hermansen, L. Effect of metabolic changes on force generation in skeletal muscle during maximal exercise. Ciba Found Symp 8:75-88, 1981.

Hermansen, L.; Hultman, E.; Saltin, B. Muscle glycogen during prolonged severe exercise. Acta Physiol Scand 71:129-139, 1967.

Holmes, C.S.; Koepke, K.M.; Thompson, R.G. Simple versus complex performance impairments at three blood glucose levels. Psychoneuroendocrinology 11(3):353-357, 1986.

Houmard, J.A.; Shinebarger, M.H.; Dolan, P.L.; Leggett-Frazier, N.; Bruner, R.K.; McCammon, M.R.; Israel, R.G.; Dohm, G.L. Exercise training increases GLUT-4 protein concentration in previously sedentary middle-aged men. Am J Physiol 264:E896-E901, 1993.

Hultman, E. Studies on muscle metabolism of glycogen and active phosphate in man with special reference to exercise and diet. Scand J Clin Lab Invest 19(Suppl 94):1-63, 1967.

Hunt, J.N. The osmotic control of gastric emptying. Gastroenterology 41:49-51, 1961.

Hunt, J.N. The site of receptors slowing gastric emptying in response to starch in test meals. J Physiol 154:270-276, 1960.

Hunt, J.N.; Knox, M.T. Regulation of gastric emptying. In: Handbook of Physiology – Alimentary Canal IV. Washington, D.C.: American Physiological Society, 1968, pp. 1917-1935.

Hunt, J.N.; Spurrell, W.R. The pattern of emptying of the human stomach. J Physiol 113:157-168, 1951.

Hunt, J.N.; Stubbs, D.F. The volume and energy content of meals as determinants of gastric emptying. J Physiol 245(1):209-225, 1975.

Indge, K.J. and Childs, R.E. A new method for deriving steady state rate equations suitable for manual or computer use. Biochem J 155:567-570, 1976.

Jacobs, I.; Kaiser, P.; Tesch, P. Muscle strength and fatigue after selective glycogen depletion in human skeletal muscle fibers. Eur J Appl Physiol 46(1):47-53, 1981.

Jenkins, D.J.A.; Thomas, D.M.; Wolever, M.S.; Taylor, R.H.; Baker, H.; Hashmein Fielden, S.R.D.; Baldwin, J.M.; Bowling, A.C.; Newman, H.C.; Jenkins, A.L.; Goff, D.V. Glycemic index of foods: a physiological basis for carbohydrate exchange. Am J Clin Nutr 34:362-366, 1981.

Linder M.C. Nutritional Biochemistry and Metabolism. New York: Elsevier, 1994, p. 39.

Margaria, R.; Aghem, P.; Rovelli, E. Measurement of muscular power (anaerobic) in man. J Appl Physiol 21:1662-1664, 1966.

Marriott, B.M. (ed). Not Eating Enough: Overcoming Underconsumption of Military Operational Rations. Washington, D.D.: National Academy Press, 1995.

McHugh, P.R.; Moran, T.H. Calories and gastric emptying: a regulatory capacity with implications for feeding. Am J Physiol 236:R254-R260, 1979.

Michaelis, L.; Menton, M.L. Die Kinetik ver Invertinwirkung. Biochem Z 49:333-369, 1913.

Moran, T.H.; McHugh, P.R. Distinctions among three sugars in their effects on gastric emptying and satiety. Am J Physiol 241:R25-R30, 1981.

Morgan, H.E., Henderson, M.J., Regen, D.M. Regulation of glucose uptake in muscle. J Biol Chem 236: 253-262, 1961.

Newsholme, E.A.; Blomstrand, E.; Ekblom, B. Physical and Mental Fatigue: metabolic mechanisms and importance of plasma amino acids. Br Med Bull 48:477-495, 1992.

Newsholme, E.A.; Leech, A.R. Biochemistry for the Medical Sciences. New York: John Wiley and Sons, 1983.

Owens, D.S.; Parker, P.Y.; Benton, D. Blood glucose and subjective energy following cognitive demand. Physiol Behav 62(3):471-478, 1997.

Pappenheimer, J.R.; Reiss, K.Z. Contribution of solvent drag through intercellular junctions to absorption of nutrients by the small intestine of the rat. J Membr Biol 100:123-136, 1987.

Parker, P.Y.; Benton, D. Blood glucose levels selectively influence memory for word lists dichotically presented to the right ear. Neuropsychologia 33(7):843-854, 1995.

Ploug, T.; Galbo, H.; Richter, E.A. Contraction induced glucose transport in skeletal muscle: Additive effect of insulin and monoexponential glycogen independent reversal in slow and fast twitch red muscle. Clin Physiol 5(Suppl 4):68, 1985.

Ploug, T.; Galbo, H.; Richter, E.A. Increased muscle glucose uptake during contractions: no need for insulin. Am J Physiol 247: E726-E731, 1984.

Rehrer, N.J.; Beckers, E.; Brouns, F; Ten Hoor, F.; Saris, W.H.M. Exercise and training effects on gastric emptying of carbohydrate beverages. Med Sci Sports Exerc 21:540-549, 1989.

Rehrer, N.J.; Wagenmakers, A.J.M.; Beckers, E.J.; Halliday, D.; Leiper, J.B.; Brouns, F.; Maughan, R.J.; Westerterp, K.; Saris, W.H.M. Gastric Emptying, absorption and carbohydrate oxidation during prolonged exercise. J Appl Physiol 72(2):468-475, 1992.

Rennie, M.J.; Jennett, S.; Johnson, R.H. The metabolic effects of strenuous exercise: a comparison between untrained subjects and racing cyclists. Q J Exp Physiol 59:201-212, 1974.

Richter, E.A.; Sonne, B.; Ploug, T.; Kjaer, M.; Mikines, K.; Galbo, H. Regulation of carbohydrate metabolism in exercise. In: Biochemistry of Exercise VI, B. Saltin, ed. Champaign, Illinois: Human Kinetics Publishers, 1986, pp. 151-166.

Schedl, H.P.; Maughan, R.J.; Gisolfi, C.V. Intestinal absorption during rest and exercise: implications for formulating an oral rehydration solution. Med Sci Sports Exerc 26:267-280, 1994.

Seiple, R.S.; Vivian, V.M.; Fox, E.L.; Bartels, R.L. Gastric-emptying characteristics of two glucose polymer-electrolyte solutions. Med Sci Sports Exerc 15(5):366-369, 1983.

Shepherd, J.T.; Vanhoutte, P.M. The Human Cardiovascular System. New York: Raven Press, 1980.

Shi, X.; Summers, R.W.; Schedl, H.P.; Flanagan, S.W.; Chang, R.; Gisolfi, C.V. Effects of carbohydrate type and concentration and solution osmolality on water absorption. Med Sci Sports Exerc 27(12):1607-1615, 1995.

Sole, C.C.; Noakes, T.D. Faster gastric emptying for glucose-polymer and fructose solutions than for glucose in humans. Eur J Appl Physiol 58:605-612, 1989.

Stryer, L. Biochemistry, 4th Ed. New York: W.H. Freeman and Co.,1995.

Taub, I.A.; Ross, E.W.; Skibinski, T.; Lieberman, H.R..; Lammi, E.; Soares, R.; Hoyt, R.W.; Fulco, C.S.; Lewis, S.F.; Staab, J. Enhancing soldier endurance with dietary carbohydrates: a physiological insight. Proceedings of the Army Science Conference, Washington, D.C., 1998.

Terjung, R.L.; Baldwin, K.M.; Winder, W.W.; Holloszy, J.O. Glycogen repletion in different types of muscle and in liver after exhausting exercise. Am J Physiol 226: 1387-1391, 1974.

Thomas, D.E.; Brotherhood, J.R.; Brand, J.C. Carbohydrate feeding before exercise: effect of glycemic index. Int J Sports Med 12(2):180-186, 1991.

Tinker, J.; Kocak, N.; Jones, T.; Glass, H.I.; Cox, A.G. Supersensitivity and gastric emptying after vagotomy. Gut 11:502-505, 1970.

Torsdottir, I.; Alpsten, M.; Andersson, D.; Brummer, R.J.M.; Andersson, H. Effect of different starchy foods in composite meals on gastric emptying rate and glucose metabolism. 1. comparisons between potatoes, rice, and white beans. Hum Nutr: Clin Nutr 38C:329-338, 1984.

Vist, G.E.; Maughan, R.J. Gastric emptying of ingested solutions in man: effect of beverage glucose concentration. Med Sci Sports Exerc 26(10):1269-1273, 1994.

Wahren, J.; Felig, P.; Ahlborg, G.; Jorfeldt, L. Glucose metabolism during leg exercise in man. J Clin Invest 50:2715-2725, 1971.

Wahren, J.; Felig, P.; Hendler, R.; Ahlborg, G. Glucose and amino acid metabolism during recovery after exercise. J Appl Physiol 34:838-845, 1973.

Wasserman, D.H.; Vranic, M. Interaction between insulin, glucagon, and catecholamines in the regulation of glucose production and uptake during exercise. In: Biochemistry of Exercise VI, B. Saltin, ed. Champaign, Illinois: Human Kinetics Publishers, 1986, pp. 167-179.